Top Curr Chem (Z) (2016) 374:47
DOI 10.1007/s41061-016-0048-9

REVIEW

The Rise of Near-Infrared Emitters: Organic Dyes, Porphyrinoids, and Transition Metal Complexes

Andrea Barbieri[1] · Elisa Bandini[1] · Filippo Monti[1] · Vakayil K. Praveen[2] · Nicola Armaroli[1]

Received: 22 April 2016 / Accepted: 20 June 2016 / Published online: 19 July 2016

Abstract In recent years, the interest in near-infrared (NIR) emitting molecules and materials has increased significantly, thanks to the expansion of the potential technological applications of NIR luminescence in several areas such as bioimaging, sensors, telecommunications, and night-vision displays. This progress has been facilitated by the development of new synthetic routes for the targeted functionalization and expansion of established molecular frameworks and by the availability of simpler and cheaper NIR detectors. Herein, we present recent developments on three major classes of systems—i.e., organic dyes, porphyrinoids, and transition metal complexes—exhibiting the maximum of the emission band at $\lambda > 700$ nm. In particular, we focus on the design strategies that may increase the luminescence efficiency, while pushing the emission band more deeply in the NIR region. This overview suggests that further progress can be achieved in the near future, with enhanced availability of more robust, stronger, and cheaper NIR luminophores.

Keywords Near-infrared luminescence · Organic dyes · Porphyrinoids · Transition metal complexes

This article is part of the Topical Collection "Photoluminescent Materials and Electroluminescent Devices"; edited by Nicola Armaroli and Henk Bolink.

✉ Vakayil K. Praveen
vkpraveen@niist.res.in

✉ Nicola Armaroli
nicola.armaroli@isof.cnr.it

[1] Istituto per la Sintesi Organica e la Fotoreattività, Consiglio Nazionale delle Ricerche (ISOF-CNR), Via Gobetti 101, 40129 Bologna, Italy

[2] Photosciences and Photonics Section, Chemical Sciences and Technology Division, National Institute for Interdisciplinary Science and Technology (CSIR-NIIST), Thiruvananthapuram, Kerala 695019, India

1 Introduction

Luminescence is a physical phenomenon of wide-ranging and increasing importance [1]. Life itself on our planet is sustained by light emission from the outer shell of the sun as a result of a complex chain of absorption/emission events triggered by γ-rays emitted upon nuclear fusion processes [2]. In our modern daily lives, we take advantage of several light emitting devices, for instance when we switch on artificial lights, watch the screen of a telephone or a computer, or check out at the supermarket.

Luminescence can be defined as the generation of light by matter through the formation of transient electronically excited states which, partially or totally, deactivate through emission of electromagnetic radiation in the visible (Vis) and near-infrared (NIR) spectral regions. Such states can be produced through a variety of stimuli such as light (photoluminescence), voltage (electroluminescence), heat (thermoluminescence), electrons (cathodoluminescence), chemical potential (chemiluminescence), mechanical action (piezo/triboluminescence), acoustic waves (sonoluminescence), and ionizing radiation (radioluminescence). Each of these subfields entails extensive scientific exploration, sometimes at the frontier of knowledge, and a wealth of technological applications ranging from lighting to telecommunications and from lasers to the investigation of biological environments [3]. In the latter area, luminescence has become a very successful analytical tool due to the exceptional sensitivity and low toxicity compared to, for instance, methods based on radionuclides [4, 5]. In the area of photochemical sciences, luminescence is perhaps the most powerful tool to trace the generation and fate of electronic excited states produced by light stimulation [6]. This affords key kinetic information to optimize functional supramolecular systems or nanomaterials for specific applications such as solar energy conversion.

The vast majority of luminescent molecules and materials produced and investigated in the last decades emits in the visible spectral region, from violet to red [6]. This trend has been driven by several factors: (1) the main practical applications (e.g., light sources, displays) require an emission output detectable by the human eye; (2) plenty of robust and cheap photodetectors for Vis detection are available, making basic scientific instrumentation generally affordable; (3) according to the energy gap law, luminescence quantum yields tend to decline by decreasing the emission energy [7], therefore NIR detection is typically more challenging than Vis; (4) high sensitivity detectors for low-energy NIR light need to be cooled down at cryogenic temperatures to limit background noise, hence NIR instrumentation is typically more complex and substantially more expensive to buy and maintain compared to Vis apparatuses.

In recent years, a marked change has occurred and NIR luminescence has moved out from obscurity to become a quickly expanding and increasingly popular field of investigation [8–10]. This has been driven by the availability of more affordable and sensitive NIR detectors and, even more, by the expansion of some technological fields in which NIR luminescence is a perfect tool for analytical detection and transmission of information. This applies in particular to imaging in biological

environments [10], which are much more transparent to NIR than Vis radiation and to telecommunications via fiber optics, which transmit NIR photons with very high efficiency [11].

We present herein three selected classes of NIR emitting molecules (i.e., with $\lambda_{max} \geq 700$ nm) that have emerged in the last two decades, namely organic dyes, porphyrinoids, and transition metal complexes. Our aim is to highlight recent trends in molecular design to enhance emission performance, which may drive future developments in a field of research that is clearly poised to expand in the years to come. The reader may refer to recent literature for other established or emerging classes of NIR emitting materials and molecules, such as metal complexes of trivalent lanthanide ions (e.g., Yb, Nd, Er) [11], fused polycyclic aromatic compounds [12], core-enlarged perylene dyes [13], semiconducting single-walled carbon nanotubes [14, 15], quantum dots and other nanomaterials [16, 17], which are not examined in the present review.

2 Organic Emitters

Molecules of fascinating colors are popular as dyes and are widely used in staining. Recently, extensive use of dyes in advanced applications, such as ink-jet printing, imaging, and in electronics, has expanded substantially. This trend helped chemists to widen the search of next-generation functional dyes. In particular, a great deal of interest is concentrated on dyes whose absorption and/or emission lies within the NIR spectral region ranging from 750 to 2000 nm, which may lead to advanced applications in night-vision target identification, information security display, bio-imaging, and sensors [18–22]. Besides this, it is well admitted that the materials used in solar cells should have good light-harvesting capability starting from the UV–Vis spectral range to the NIR range, as sunlight possesses 50 % of its radiation energy in the IR region. Though NIR-emissive organic materials (emitting beyond 750 nm) are far less common than NIR-absorbing organic materials, they are well known for their potential applications in telecommunications, displays, and bio-imaging [18–22]. They are particularly interesting for the latter use, because biological environments have typically no autofluorescence in the NIR and tissues are virtually transparent in the window between 750 and 900 nm. In this section, we review some of the recent developments related to NIR fluorescent organic molecules.

2.1 Cyanines

The basic structural motif of classical cyanine dyes is a polymethine chain bridging two aromatic nitrogen-containing heterocycles (Fig. 1a) [20, 21]. One of the merits of cyanine dyes is that their optical properties can be tuned from Vis to NIR by changing the number of methine groups in the bridging chain [18, 19, 21, 22]. The addition of each vinylene group introduces nearly a 100-nm bathochromic shift, thus the emission wavelength of heptamethine cyanine reaches well into the NIR region

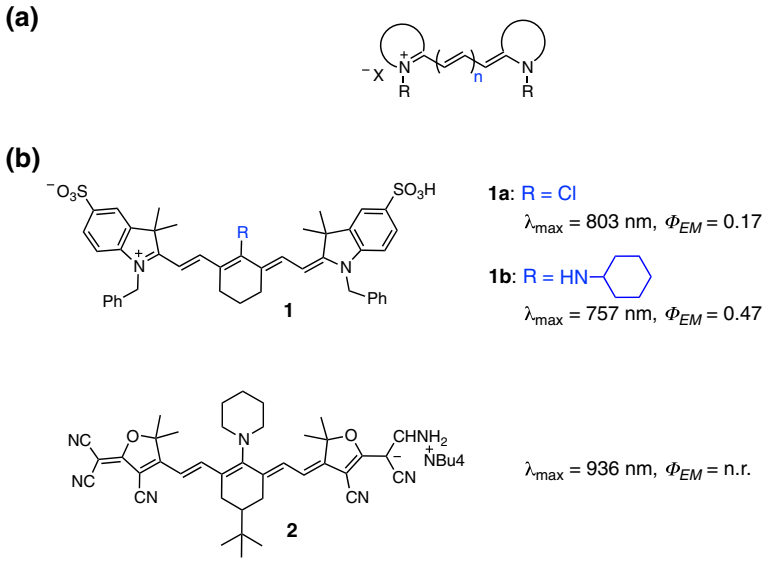

Fig. 1 **a** General structure of cyanine dyes, **b** chemical structures of NIR-emitting cationic and anionic cyanines. Data for cationic and anionic cyanines, respectively, refer to aqueous and CH_2Cl_2 solution at room temperature

[18, 19, 21, 22]. Cyanine dyes, characterized by narrow absorption band and high molar extinction coefficients ($>10^5$ M^{-1} cm^{-1}), are weakly luminescent due to the flexibility of the polymethine bridge that undergoes isomerization in the excited state [18, 19, 21]. Introduction of chlorocyclohexenyl group as a part of the polymethine chain (**1a**, Fig. 1b) has been found to stiffen the backbone, thereby improving quantum yield ($\lambda_{max} = 803$ nm, $\Phi_{EM} = 0.17$) as well as photostability [20, 21, 23]. The replacement of the chloro group of cyclohexenyl moiety with substituted amine enables heptamethine cyanine dye **1b** (Fig. 1b) to display a large Stokes shift (155 nm) and NIR emission with very good quantum yield ($\lambda_{max} = 757$ nm, $\Phi_{EM} = 0.47$) due to the excited state intramolecular charge transfer occurring between the donor and acceptor moieties in the dye [23]. The photostability of these dyes is further improved by reducing the electron density at the amine moieties by introducing electron-withdrawing groups such as the acetyl residue exhibiting superior performance in in vivo studies compared to other commercial NIR dyes [23]. Introduction of electron-donating groups at the N-atom of aromatic heterocycles is also found to improve the photostability of NIR-emitting cyanine dyes [24]. Furthermore, intramolecular crosslinking of the 1,1′ position (N-atom of aromatic heterocycle) of classical heptamethine dyes has been found to enhance the photo and thermal stabilities [25]. Thus, cyanines are considered an excellent platform in the design of probes useful for the detection and imaging of various analytes such as metal ions, anions, pH, enzymes, thiols, reactive oxygen, and nitrogen species [18, 19, 22].

In general, cyanine dyes are cationic, an exception of this is the anionic dye featuring tricyanofuran terminal groups **2** (Fig. 1b) [26]. Compared to the analogues cationic cyanine dye, the anionic dye shows red-shifted absorption ($\lambda_{abs} = 900$ nm) and emission ($\lambda_{max} = 915$ nm) with very good thermal stability, which makes it suitable for bioimaging applications.

2.2 Pyrrolopyrrole Cyanines

Pyrrolopyrrole cyanine (PPCy) dyes are new members of the family of cyanine-type dyes but, unlike the parent molecules, they are nonionic [27–30]. PPCy systems show good absorption in the NIR region but, however, are nonluminescent due to torsional vibration mediated nonradiative decay of the excited state [27, 28]. This issue has been circumvented by stiffening the chromophore through chelation with BF_2 and BPh_2, which strongly reduces radiationless decay pathways and makes them highly fluorescent (Fig. 2) [27, 28]. The luminescence quantum yield values observed for the dyes **3a** and **3b** ($\Phi_{EM} = 0.32$–0.69) are exceptional for NIR fluorophores. Studies have shown that the optical properties of PPCy dyes can be tuned in a wide spectral range by changing the terminal heteroaromatic substituents [28]. Interestingly, some of the derivatives of PPCy dyes such as the BF_2 and BPh_2 chelated bis(pyrrolopyrrole) cyanines **4a** and **4b** (Fig. 2) exhibit strong fluorescence in the spectral region close to 1 μm [29]. The design of asymmetric NIR-emitting BF_2 chelated PPCy has allowed biofunctionalization of the dye and its utilization for live cell imaging [30].

2.3 Squaraines

Squaraines belong to the class of polymethine dyes with resonance-stabilized zwitterionic structures [31–38]. Squaraine dyes are characterized by a donor–

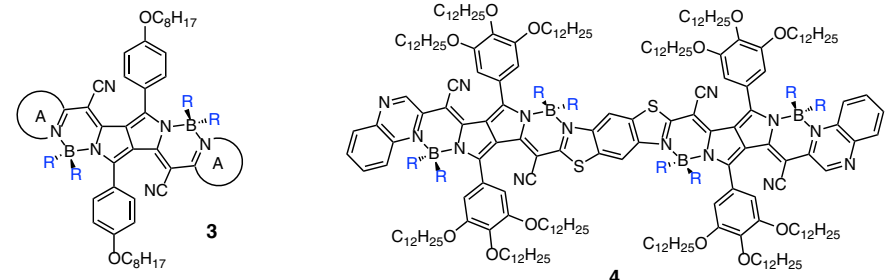

Fig. 2 Chemical structure of NIR-emitting BF_2 and BPh_2-chelated PPCy dyes. All the data refer to $CHCl_3$ solution at room temperature

acceptor–donor type substitution pattern that consists of electron-rich aromatic or heterocyclic moieties on both sides of an electron-deficient oxocyclobutenolate core. In general, the optical properties of squaraine dyes are quite similar to cyanine dyes. However, the unique combination of photostability and optical properties that reach the NIR region make squaraines attractive for nonlinear optics, molecular recognition, biolabeling and imaging, photodynamic therapy, bulk heterojunction, and dye-sensitized solar cells [31, 32, 34–39]. Although squaraine dyes show intense and sharp optical features in solution, the strong propensity to aggregate and the susceptibility of the central cyclobutene ring to undergo chemical attack are considered as drawbacks. The physical encapsulation of squaraine dyes in tetralactam macrocycles has been found to overcome these issues [34]. Based on this approach, a variety of stable NIR-emissive squaraine dyes that can be used in in vivo imaging has been developed [34].

It has been demonstrated that the optical properties of squaraine dyes can be pushed to the NIR region by extending the conjugation length as well as increasing the strength of the donor moiety conjugated with the central core [32–37]. The recent finding of the unusual halogen effect in the NIR-emitting properties of squaraines is particularly interesting [40, 41]. The dicyanovinyl functionalized squaraines **5** and **6** (Fig. 3) exhibit a bathochromic shift in absorption and emission properties with an increase in molar extinction coefficient and fluorescence quantum yield depending on substituents H < Cl < Br < I (Fig. 3). This trend is against the common perception of the effect of heavy atoms on the fluorescence properties of squaraines, which are known to quench the luminescence by favoring the intersystem crossing through strong spin–orbit coupling [36]. Detailed optical, crystallographic, and computational studies showed that the high-fluorescence quantum yield values of squaraines even in the NIR region are due to the stiffening of the structure, as their central four-membered ring restrains the conjugated backbone of the molecule in the cisoid conformation (Fig. 3) [40, 41]. The observed halogen effects on the optical properties is correlated with the polarizability of halogen substituents, which, in fact, determine the transfer of electron density from the substituents to the chromophore core.

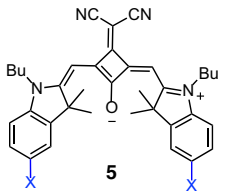

5

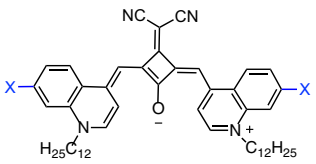

6

5a: X = H λ_{max} = 698 nm, Φ_{EM} = 0.37

5b: X = Cl λ_{max} = 708 nm, Φ_{EM} = 0.47

5c: X = Br λ_{max} = 710 nm, Φ_{EM} = 0.47

5d: X = I λ_{max} = 713 nm, Φ_{EM} = 0.58

6a: X = H λ_{max} = 890 nm, Φ_{EM} = 0.10

6b: X = Cl λ_{max} = 913 nm, Φ_{EM} = 0.11

6c: X = Br λ_{max} = 916 nm, Φ_{EM} = 0.12

6d: X = I λ_{max} = 922 nm, Φ_{EM} = 0.17

Fig. 3 Chemical structure of NIR-emitting dicyanovinyl functionalized squaraines. All the data refer to CH_2Cl_2 solution at room temperature

2.4 BODIPYs

Borondipyrromethenes (BODIPYs) can be considered as rigid cross-conjugated cyanine dyes (Fig. 4). These dyes display narrow and structured optical features with high molar extinction coefficients and relatively small Stokes shifts. The spectroscopic properties of these dyes have been found less influenced by environment factors such as solvent polarity and pH [42–46]. BODIPYs are well appreciated for their ability to fluoresce with high quantum yields approaching unity [42–46]. This excellent emission performance of BODIPY dyes is attributed to the presence of boron atoms in the polymethine chain, which introduces rigidity to the molecule and strongly limits non-radiative decays of the excited state through *trans–cis* isomerization and twisting. The combination of properties of BODIPY dyes makes them a useful platform to design NIR-emitting molecules [18, 19, 22, 46].

In general, the pristine BODIPY core exhibits the lowest energy absorption and emission features at around 500 nm [42, 43]. Over the years, a number of strategies have been developed to shift the optical properties of BODIPYs in the far-red and NIR regions (Fig. 4) [12, 19, 22, 42, 44, 47, 48]. These approaches mainly aim at extending the conjugation length and lowering the resonance energy, including (1) attachment of a styryl or ethynyl phenyl substituent to the 3 and/or 5-positions, (2) fusion of a rigid aromatic ring to the pyrrole unit, (3) replacement of *meso* carbon with a nitrogen atom to form aza analogues, and (4) introduction of polycyclic aromatic compound at the *meso* position [12, 19, 22, 38, 42, 44, 47, 48]. Apart from these methods, the attachment of thiophene at 1-, 3-, 5-, and 7-positions of the aza-BODIPY has demonstrated to red shift the absorption ($\lambda_{abs} = 733$ nm) and emission ($\lambda_{max} = 757$ - nm) in comparison to the phenyl-substituted derivative ($\lambda_{abs} = 643$ nm, $\lambda_{max} = 673$ - nm) [49]. The origin of the bathochromic shift is ascribed to the reduction of torsion angles and the increase of electron donation to the aza-BODIPY core, when the thienyl group replaced the phenyl substituents. Grafting of short oligomeric thiophene units to the 3,5-positions of BODIPY has shown to tune the emission maxima of the dye from 640 ($\Phi_{EM} = 0.78$) to 769 nm ($\Phi_{EM} = 0.14$) in CH_2Cl_2 solution [50].

2.5 Rhodamines

Rhodamine dyes are excellent orange-red-emitting chromophores having good photostability [51, 52]. These dyes have been used extensively for the design of fluorescent probes and labeling agents [22, 51, 52]. Recently, few new approaches have been developed to shift their emission maxima in the NIR region with a view

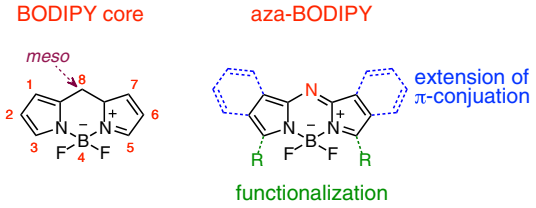

Fig. 4 Different molecular approaches used to shift the optical properties of BODIPY in the NIR region

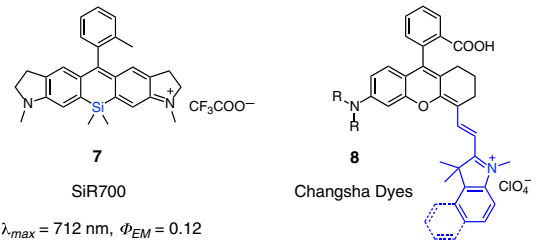

Fig. 5 Chemical structures of Si-rhodamine **7** and Changsha dyes **8** showing NIR emission

to utilize them in bioimaging [53–55]. The chemical modifications on the xanthene core such as replacement of oxygen with silicon has been found to be an effective method to develop NIR-emitting rhodamine analogues (**7**, Fig. 5) [53, 54]. The bathochromic shift of the optical properties of Si-rhodamine derivatives **7** (Fig. 5) compared to the classical rhodamine dyes is attributed to the relatively low lying lowest unoccupied molecular orbital (LUMO) energy levels. This effect is facilitated by σ*–π* conjugation, which results from the σ* orbital of silicon–carbon (exocyclic methyl groups) and the π* orbital of the adjacent conjugated carbon atoms. In a different approach, a new series of dyes known as Changsha NIRs (**8**, Fig. 5) have been developed. The objective is the combination of the spirocyclization-based luminescence on–off switching exhibited by classical rhodamines with merocyanines, which are NIR dyes [55]. Changsha NIRs **8** exhibit strong emission in the NIR region (λ_{max} = 721–763 nm) with relatively good quantum yield values (Φ_{EM} = 0.29–0.56) in ethanol.

2.6 Donor–Acceptor Substituted Chromophores

An appealing strategy to develop chromophores with optical properties in the NIR region is linking electron donor (D) and acceptor (A) molecular units through a conjugated π-spacer (Fig. 6) [19, 21]. The D-π-A-π-D substitution pattern has been found to enhance the electronic communication between the donor and acceptor moieties and thus considerably reduce the band gap energy [19, 21, 56–59]. The NIR optical features of such chromophores are determined by the strength of the donor–acceptor units, the choice of conjugated π-spacer, and the combination thereof. The most commonly used donor units includes diarylamine, thiophene, and fluorene, and the acceptor units are mainly heterocycles such as derivatives of benzo *bis*(1,2,5-thiadiazole) and diketopyrrolopyrrole. Electron-rich π-spacers such as thiophene and pyrrole are preferable over phenyl because they facilitate quinonoid structure formation and intramolecular charge transfer. In Fig. 6 are reported three families of molecules (**9**–**11**), which exemplify this strategy [56].

3 Porphyrinoids

Porphyrins are conjugated tetrapyrrolic macrocycles, which exhibit remarkable chromophoric, luminophoric, and electrochemical properties [60]. They are considered "the pigments of life" due to their wide presence in biological

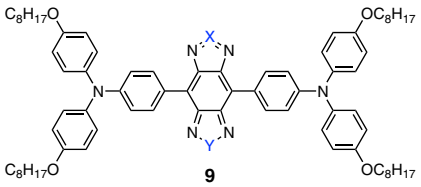

9

9a: X, Y = S λ_{max} = 1065 nm, Φ_{EM} = 0.071

9b: X = Se, Y = S λ_{max} = 1120 nm, Φ_{EM} = 0.028

9c: X, Y = Se λ_{max} = 1230 nm, Φ_{EM} = 0.018

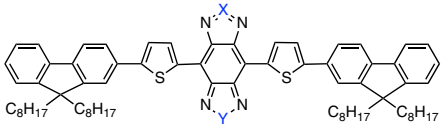

10

10a: X, Y = S λ_{max} = 1055 nm, Φ_{EM} = 0.185

10b: X = Se, Y = S λ_{max} = 1120 nm, Φ_{EM} = 0.046

10c: X, Y = Se λ_{max} = 1285 nm, Φ_{EM} = 0.019

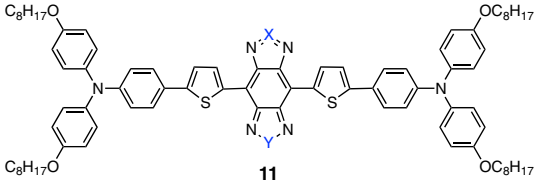

11

11a: X, Y = S λ_{max} = 1125 nm, Φ_{EM} = 0.053

11b: X = Se, Y = S λ_{max} = 1295 nm, Φ_{EM} = 0.011

11c: X, Y = Se λ_{max} = 1360 nm, Φ_{EM} < 0.01

Fig. 6 Chemical structures of NIR-emitting D-π-A-π-D chromophores. All the data refer to toluene solution at room temperature

environments where, for instance, serve as light harvesting units or oxygen carriers. As robust and versatile molecular platforms, they can be easily functionalized to afford multichromophoric systems [61]. Moreover, they can undergo a variety of supramolecular interactions, via π-stacking [62], charge-transfer [63], and metal–ligand interactions [64], occurring both in solution and on surfaces [65]. Due to this outstanding combination of properties, it is not surprising that porphyrins have been one of the most investigated classes of molecules over the last decades.

Porphyrin-related systems are generally termed "porphyrinoids", a vast family of molecules that includes both naturally occurring and, to an increasing extent, synthetic macrocyclic molecules with pyrrole units [66, 67]. The remarkable and strongly tunable chromophoric and luminophoric properties of porphyrinoids, as a

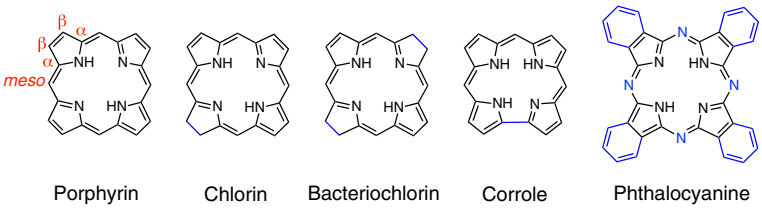

Fig. 7 The basic structure of the most important porphyrinoids. For porphyrins, the conventional names of the ring positions in which substituents can be inserted are indicated. The structural variations with respect to the pristine porphyrin structure are highlighted in *blue*

function of the specific chemical structure and connectivity, make them interesting for photonic, analytical, and therapeutic applications [68]. In particular, some "free base" and metallated porphyrinoids are among the strongest NIR emitters available to date, and their number continues to increase. The basic skeleton of the most important families of porphyrinoids is depicted in Fig. 7.

3.1 Standard and Extended Porphyrins

The photophysical properties of porphyrins—both free base and metallated—have been investigated since the 1960s [69]. Typically, they exhibit a very intense absorption feature between about 400 and 450 nm (the so-called Soret band, or B-band) that corresponds to the transition to the second singlet excited state ($S_0 \rightarrow S_2$). At lower energy (500–700 nm), an envelope of weaker characteristic absorption features occurs, related to the $S_0 \rightarrow S_1$ transitions (Q bands). Both bands have a π–π^* character and their very different intensities and energies are explained in detail by the so-called Gouterman four orbital model [69].

The prototypical free base tetraphenyl porphyrin (H_2TPP) exhibits fluorescence in the visible spectral region ($\lambda_{max} = 646$ nm) and chemical substitution do not remarkably affect this behavior [70]. Upon complexation with closed-shell diamagnetic ions—e.g., Zn(II), Cd(II), Mg(II), Al(III)—[71, 72] fluorescence in the visible spectral region is also observed, with moderate-to-low quantum yields. H_2TPP and related metalloporphyrins also exhibit phosphorescence bands in the NIR region (e.g., ZnTPP: $\lambda_{max} = 776$ nm, toluene matrix) [73] but they are typically weak and observable only in rigid matrix at cryogenic temperatures [71], hence their interest is limited. The triplet excited state lifetime is in the range of ms and, in solution, can only be detected by transient absorption upon removal of oxygen [74].

Taking advantage of heavy atom effects, the porphyrin triplet excited state lifetime can be shortened below the ms threshold. Accordingly, triplet emission at room temperature is observable in porphyrins of second- and third-row transition metals, such as Ru(II) and Os(II), which saturate their octahedral coordination cage by coordinating ligands in the apical positions. A standard ruthenium porphyrin system exemplifying the general photophysical behavior of this class of compounds is [Ru(TPP)(CO)(py)] **12** (Fig. 8) [75], which exhibits weak phosphorescence in

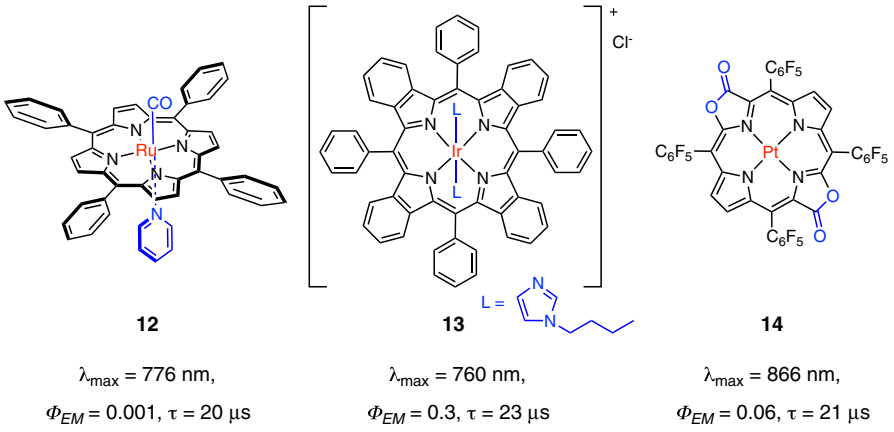

Fig. 8 Selected examples of NIR-emitting Ru(II) [75, 76], Ir(III) [78] and Pt(II) porphyrins [81]. Ru-porphyrins are faint emitters, Ir-porphyrins are rare, Pd-porphyrins can afford good yields both with ring modifications (this example, *trans*-porphodilactone) and ring expansion (see below). Photophysical data are in solution at 298 K, in toluene (Ru- and Ir-porphyrin) and CH_2Cl_2 (Pt-porphyrin)

solution at room temperature ($\lambda_{max} = 726$ nm, $\Phi_{EM} = 0.001$, $\tau = 30$ μs in deaerated toluene) [76]. In these compounds, ring-centered and charge transfer (metal-to-ring) excited states are very close in energy, and the lowest-lying one depends on specific ring substituents or axial ligands [77]. Os(II) porphyrins behave similarly to Ru(II) analogues, with weak NIR triplet emission at room temperature ($\ll 0.01$) [74].

Despite the fact that Ir(III) complexes and porphyrins have been widely investigated in recent years, iridium porphyrins are not very common, primarily because they are difficult to synthesize. One example of strongly emitting NIR Ir(III)-porphyrin **13** has been reported (Fig. 8); this compound exhibits $\lambda_{max} = 760$ nm, $\Phi_{EM} = 0.3$, $\tau = 23$ μs in deaerated toluene [78]. Corroles—smaller analogues of porphyrins with a direct C–C link between two pyrrole rings [79] (Fig. 7)—can also bind Ir(III). However, NIR emission from iridium corroles is very weak, probably due to enhanced non-radiative deactivation favored by the more distorted structure [80].

The most relevant NIR-emitting porphyrins are those based on Pt(II) and Pd(II), the former ones being probably the most successful NIR-emitting transition metal complexes in general [9]. Pt(II)- and Pd(II)-porphyrins are square planar, without additional axial ligands. They are relatively easy to synthesize and chemically modify, exhibit good photo and thermal stability, and are typically well soluble. Chemical modifications of standard Pt(II)- and Pd(II)-porphyrins can afford near-infrared emission with reasonable quantum yields [82], as also recently demonstrated with porphodilactones **14** (Fig. 8) [81].

Further progress can be expected in this area; meanwhile, the most effective strategy to obtain strong NIR luminescence is still the expansion of the ring π-conjugation [83]. This approach has been fruitfully proved by extending the conjugation of the pyrrole rings in Pt(II)-porphyrins and by investigating the effect

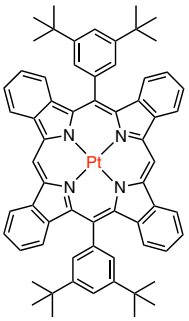

15

λ_{max} = 770 nm

Φ_{EM} = 0.49, τ = 53 µs

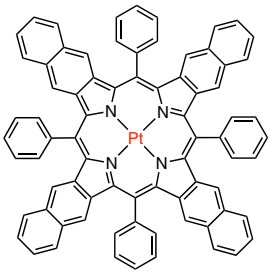

16

λ_{max} = 891 nm

Φ_{EM} = 0.15, τ = 12.7 µs

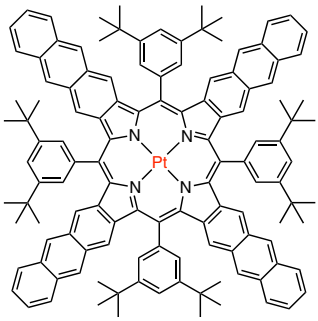

17

λ_{max} = 1022 nm

Φ_{EM} = 0.08, τ = 3.2 µs

Fig. 9 π-extended Pt(II) porphyrins with progressively NIR-shifted emission in degassed toluene solution. The photoluminescence quantum yield is maximized with two *trans* aryl substituents in the *meso* positions instead of four. Shifting photoluminescence to the NIR region is promoted by enhancing the number of fused benzene units on the pyrrole rings (from *left* to *right*)

λ_{max} = 773 nm, Φ_{EM} = 0.35, τ = 30 µs (toluene)

λ_{max} = 765 nm, Φ_{EM} = 0.70, τ = 53 µs (methylcyclohexane)

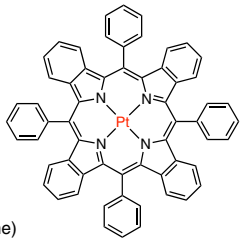

18

Fig. 10 Pt(II)-tetraphenyltetrabenzoporphyrin, a molecule successfully used to make electricity-to-light and light-to-electricity conversion devices

of the number and type of substituents in the *meso* positions [84]. As indicated in Fig. 9, these systems can achieve emission quantum yields has high as 0.49 (770 nm) (**15**) and emission bands down to 1022 nm ($\Phi_{EM} = 0.08$) (**17**), with lifetimes in the 10^{-6}–10^{-5} s range.

The emission performance of the same metalloporphyrin may differ with the solvent. An example is Pt(II)-tetraphenyltetrabenzoporphyrin **18** (Fig. 10), a molecule with a combination of remarkable properties (chemically stable, non-ionic, strong triplet NIR emitter with large Stokes' shift) that make it ideal as photoactive component in different types of optoelectronic devices. It has been used to make a NIR-emitting OLED with an external quantum efficiency above 6 % [85] and a luminescent solar concentrator with projected light-to-electricity power efficiency above 6.5 % [86]. This is probably the most promising and useful NIR emitter reported to date in terms of optoelectronic applications.

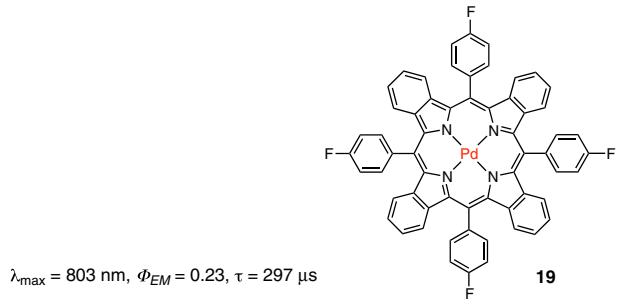

Fig. 11 Pd(II)-*meso*-tetra(4-fluorophenyl)tetrabenzoporphyrin. The data are in toluene solution at room temperature

Some examples of β-substituted [81] and π-extended [9] Pd(II)-porphyrins which emit in the NIR region have been also reported. Typically, when compared to Pt(II) analogues, Pd(II)-porphyrins exhibit red-shifted emission bands, lower phosphorescence quantum yields and longer lifetimes [81, 83, 87, 88]. The strongest NIR-emitting Pd(II)-porphyrin **19** with the lowest energy luminescence band reported to date is depicted in Fig. 11 [88]. It entails the use of fluorinated substituents, a strategy that affords enhanced luminescence performance and better stability.

3.2 Porphyrins with Expanded Rings or Modified Pyrrole Connectivity

In recent years, a great deal of work has been made in the synthesis of porphyrin-type systems with modified structure. Two main strategies have been adopted: (1) expansion of the macrocycle using more than four pyrrole units (e.g., hexaphyrin, Fig. 12) and (2) change of the linking mode between the pyrrole units, to get to a variety of tetrapyrrolic porphyrin variants (Fig. 12).

Expanded porphyrins containing up to ten pyrrole units have been synthesized [89, 90]. These π-conjugated aromatic macrocycles typically exhibit good solubility and can bind one or even two metal ions. Due to their remarkable chromophoric and photophysical properties, they can be used as dyes, sensors, two-photon absorbing materials, or photosensitizers for photodynamic therapy [91]. They exhibit an

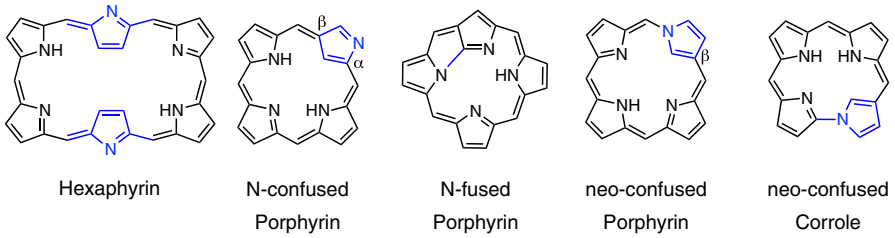

Fig. 12 An example of expanded porphyrin with a six-membered ring and four porphyrinoids with modified connectivities between the pyrrole rings. The so-called norrole (*far right*) is a corrole isomer with a C–N bond between two pyrrole units

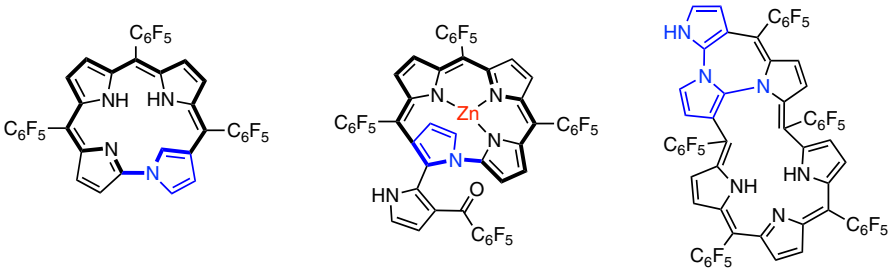

20

λ_{max} = 705 nm,

Φ_{EM} = 0.06, τ = n.r.

21

λ_{max} = 741 nm,

Φ_{EM} = 0.10, τ = n.r.

22

λ_{max} = 900 nm,

Φ_{EM} = 0.003, τ = n.r.

Fig. 13 Porphyrinoids with modified connectivity between pyrrole rings exhibiting good luminescence quantum yields (**20** and **21**) [93, 96] and neo-fused hexaphyrin **22** with weak emission at 900 nm [97]. All the data refer to CH_2Cl_2 solution at room temperature

electronic absorption profile extending into the red and near-infrared spectral region and several of them are reported to exhibit NIR luminescence [92]. However, due to strong conformational flexibility, they are prone to non-radiative deactivation and emission quantum yields are poor (<1 % [93]) and often not reported, presumably due to signal weakness [92, 94].

As far as tetrapyrrole porphyrin rings with modified connectivity are concerned (Fig. 12), some are reported to be poor NIR emitters ($\Phi_{EM} = 10^{-4}$–10^{-6}) [95], but others exhibit good luminescence such as those depicted in Fig. 13 [93, 96]. These molecules have fluorinated substituents in the *meso* positions, a successful strategy to reduce non-radiative deactivations proposed also for other porphyrin systems [88]. More recently, the two-ring modification approaches have been merged to obtain "expanded" and "confused" porphyrinoids such as **22** (Fig. 13), which emits at 900 nm with very low quantum yield [90, 97].

3.3 Bacteriochlorins

Chlorins (also termed dihydroporphyrins) are macrocycles made of three pyrroles and one 1-pyrroline unit, which normally exhibit luminescence in the red-spectral region. This large family of compounds includes chlorophylls, i.e., magnesium containing chlorins, which constitute the central photosensitive pigments in the chloroplasts of plants and algae. Porphyrinoids made of two alternate 1-pyrroline and pyrrole units are called bacteriochlorins (or tetrahydroporphyrins), their name being related to their role as NIR light-harvesting molecules in photosynthetic bacteria (Fig. 7). By moving from porphyrins to chlorin to bacteriochlorins, the lowest energy absorption features (Q bands) move from the yellow-orange, to the red and then to the NIR spectral region [98]. Natural bacteriochlorins are not particularly stable and tend to be oxidized to chlorins or porphyrins. However, recently, new synthetic strategies have afforded stable bacteriochlorins, opening the

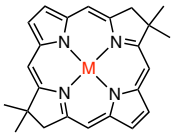

23

23a M = H2: λ_{max} = 716 nm, Φ_{EM} = 0.14, τ = 4.0 ns

23b M = Zn: λ_{max} = 725 nm, Φ_{EM} = 0.10, τ = 3.4 ns

24a M = H2: λ_{max} = 805 nm, Φ_{EM} = 0.15, τ = 3.2 ns

24b M = Zn: λ_{max} = 825 nm, Φ_{EM} = 0.17, τ = 3.6 ns

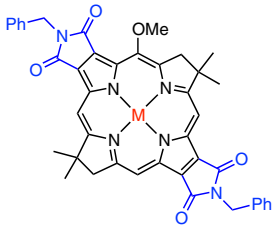

24

Fig. 14 Simple bacteriochlorins **23** and their bisimide analogues **24** with lower energy and stronger NIR emission. The geminal dimethyl residues on the reduced pyrrole units impart stability by preventing dehydrogenation. Photophysical data are in toluene at room temperature

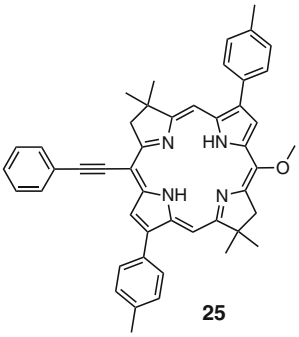

25

λ_{max} = 760 nm, Φ_{EM} = 0.19, τ = 5.7 ns

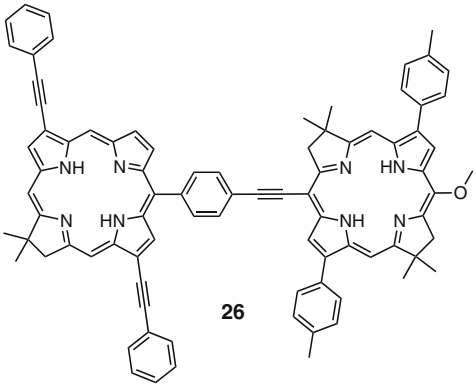

26

Fig. 15 A phenylethynil-substituted bacteriochlorin **25** (5-methoxy-15-(2-phenylethynyl)-8,8,18,18-tetramethyl-2,12-di-*p*-tolylbacteriochlorin) with NIR fluorescence in toluene at room temperature, and a related free-base chlorin dyad **26**. The emission properties of the latter, upon excitation of the chlorin moiety, are exactly the same as those of the bacteriochlorin model, indicating quantitative energy transfer in toluene solution at room temperature

route to an expanding class of NIR-emitting dyes with $\lambda_{max} > 700$ nm, in which the pristine bacteriochlorine core bears a variety of aliphatic and aromatic fragments [99], also with several coordinating metals, such as Zn(II), Mg(II), and Pd(II) [100].

The simplest synthetic free base **23a** and Zn(II)-bacteriochlorins **23b** (Fig. 14) exhibit NIR fluorescence at 716–725 nm, which is substantially red shifted (805–825 nm) and even enhanced upon fusion of the pyrrole moieties with five-membered bisimide rings (**24a–b**, Fig. 14) [101].

A synthetic bacteriochlorin **25** with moderately strong NIR fluorescence is depicted in Fig. 15 [102]. This molecule has been linked to red-emitting free base

(**26**, Fig. 15) or Zn(II)-chlorin analogues and quantitative chlorin → bacteriochlorin energy transfer has been observed [103]. Due to strong red absorption and NIR emission, these porphyrinoid dyads are prototypes for molecular imaging probes in biological environments.

3.4 Porphyrin Tapes

Following a seminal paper by Crossley and Burn [104], extended π-conjugated porphyrin systems have become a popular field of research, primarily with the aim of obtaining synthetic organic materials with unusual optical and electronic properties. A landmark result in this area was the synthesis of soluble *meso–meso*, β-β,β-β triply linked zinc(II)-oligoporphyrins arrays **27** (Fig. 16), containing up to 12 fused monomeric units [105]. The lowest energy absorption features of these molecules extend linearly as a function of the monomeric units, reaching 2500 nm for the longest dodecameric system. This reveals a surprisingly long effective conjugation length (ECL) with no saturation of electronic properties, as typically observed with most organic conjugated systems of similar size. Only the smallest dimeric tape of the series (**28**, Fig. 16) is found to exhibit NIR luminescence well above 1000 nm, but with minuscule fluorescence quantum yield and ultrashort excited state lifetime [106, 107]. Interestingly, deuteration of dimeric Zn(II) porphyrin tapes does not improve the emission performance, suggesting that the observed ultrafast deactivation rate and related poor luminescence quantum yield not only depends on the Franck–Condon factor and the energy gap law, but accessible intersections of S_0 and S_1 potential energy surfaces must occur [108].

An effective strategy to promote NIR emission is to make rigid planarized *para*-phenylene-bridged tape-like porphyrin dimers, such as those depicted in Fig. 17. In particular, non-conjugation (**29**, CPh_2 link) enables emission quantum yield of 10 % at 736 nm, which is progressively weakened and shifted to longer

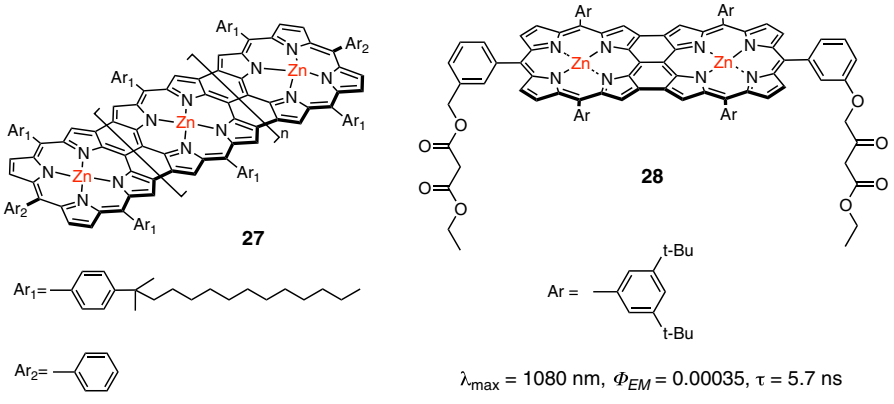

Fig. 16 *Left* β-β-linked zinc(II)-oligoporphyrin tapes **27** ($n = 0, 1, 2, 3, 4, 6, 10$). *Right* **28**, the only member of this family of compounds that exhibit (faint) luminescence. Photophysical data are in toluene solution at room temperature

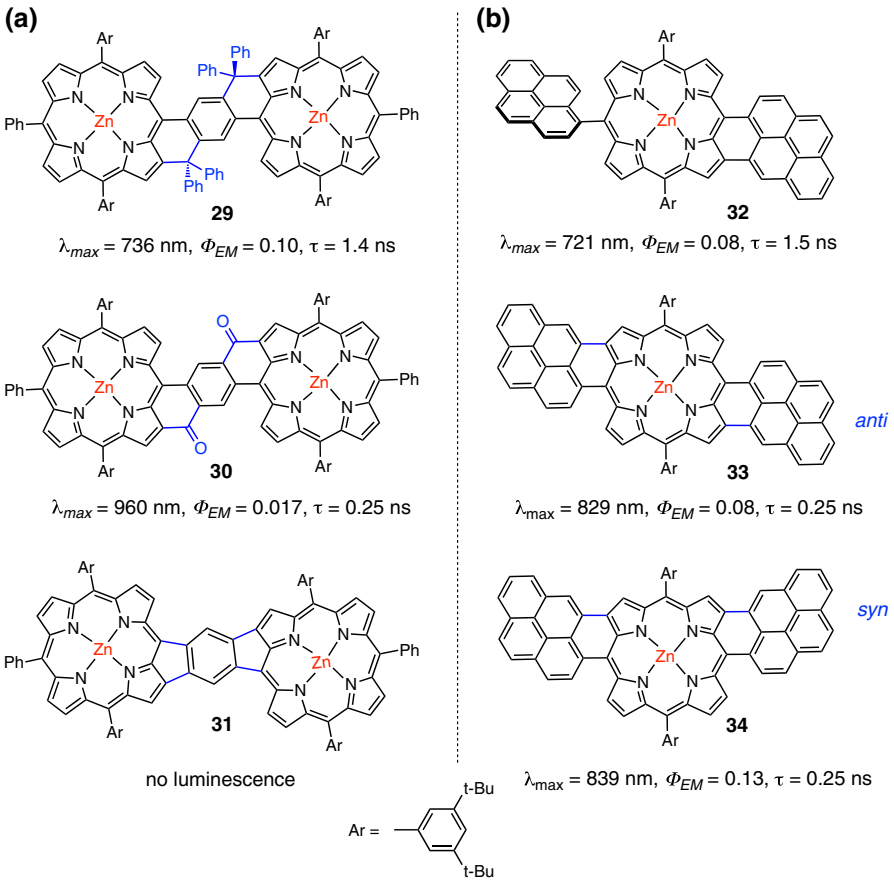

Fig. 17 **a** *Para*-phenylene-bridged Zn–porphyrin tapes, which can exhibit remarkable NIR emission in toluene solution at 298 K. **b** Molecular tapes obtained by one Zn–porphyrin unit fused with one or two pyrene moieties (CH_2Cl_2, 298 K)

wavelengths with cross-conjugation **30** (keto link), until disappearance of the luminescence when full conjugation occurs **31** (C–C link) [109] (Fig. 17a).

Even larger NIR emission quantum yields have been achieved via fusion of Zn–porphyrin rings with pyrene units (**32–34**, Fig. 17b). Besides good NIR emission, these molecules exhibit broad absorption and have good solubility; accordingly, they are of potential interest for organic photovoltaics, bioimaging, and photodynamic therapy [110]. Similar *N*-annulated perylene-fused systems exhibit photoluminescence quantum yield above 5 % at 800 nm (not shown) [111].

3.5 Linear Porphyrin Oligomers

Several linear porphyrin oligomers connected through bridges linking only the *meso* positions have been prepared. Systems with phenylene bridges are typically non-

emitting [112], whereas the direct C–C linkage affords arrays with fluorescence bands little affected with respect to the porphyrin monomer and occurring in the visible range [107]. In such arrays, the porphyrin units are perpendicularly arranged, therefore π-conjugation is disrupted and the lowest energy transition is virtually unaffected, even though exciton coupling brings about the splitting of the Soret band. Interestingly, NIR luminescence is observed when these linear porphyrin arrays **35** bear methanofullerenes as terminal units enabling face-to-face arrangements (Fig. 18), due to charge transfer (porphyrin → fullerene) interactions [113, 114]. Emission maxima are placed between 950 and 1050 nm and the intensity progressively decreases with solvent polarity, which indicates electron transfer in the Marcus inverted region [114]. The emission quantum yields have not been determined due to signal weakness and the lifetimes are in the range 500–110 ps. Anyway, such NIR emission is the most convenient spectroscopic tool for detecting such peculiar interactions.

The most interesting porphyrin arrays in terms of NIR luminescence are those connected through *meso–meso* alkyne bridges, as first demonstrated by Therien and coworkers using acetylene linkers [115]. They synthesized six Zn(II) porphyrin linear arrays (with 2, 3, or 5 subunits) with electron donating and/or accepting groups on the free *meso* position. The absorption spectra are progressively red-shifted as a function of the number of chromophores, showing that the acetylene

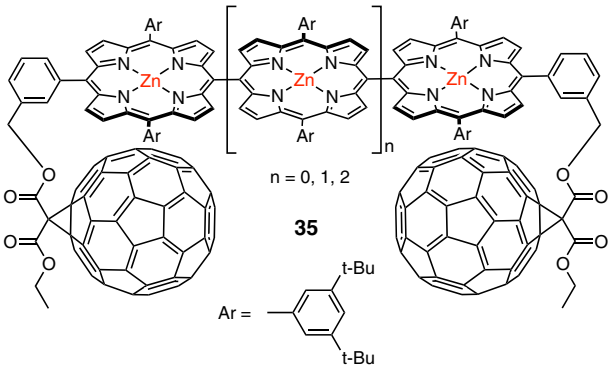

35a n=0 λ_{max} = 953 nm, τ = 0.8 ns (toluene)
λ_{max} = 1050 nm, τ = 0.4 ns (THF)

35b n=1 λ_{max} = 956 nm, τ = 0.7 ns (toluene)
λ_{max} = 1040 nm, τ = 0.3 ns (THF)

35c n=2 λ_{max} = 945 nm, τ = 1.1 ns (toluene)
λ_{max} = 1053 nm, τ = 0.4 ns (THF)

Fig. 18 Linear porphyrin arrays **35** exhibiting charge transfer emission in the NIR in apolar solvents (toluene, THF)

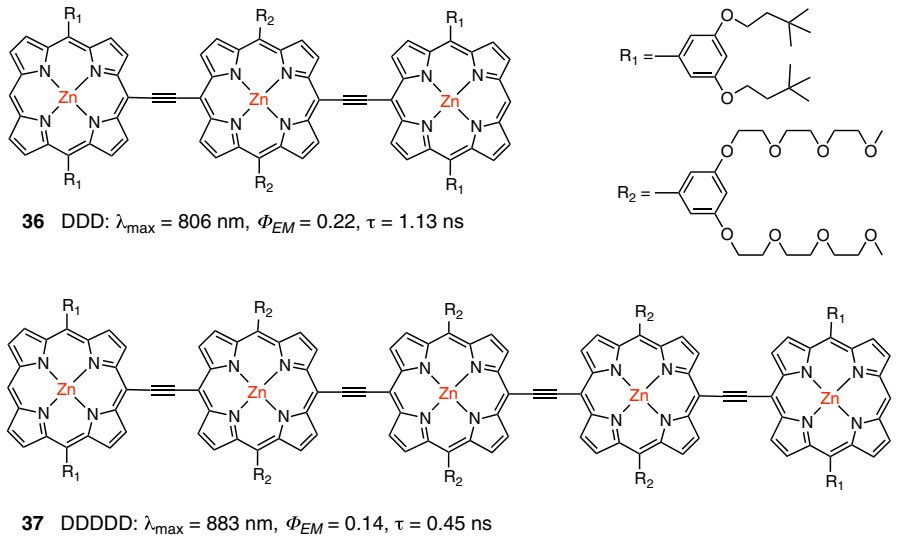

Fig. 19 Linear porphyrin arrays connected through acetylene bridges exhibiting remarkable NIR emission in THF

linker warrants effective electronic conjugation. Irrespective of the length and of the specific sequence of donors or acceptors, these systems exhibit good NIR emission, particularly when electron donor residues are used [115]. In Fig. 19 are reported the arrays exhibiting the highest luminescence quantum yield and the lowest-energy emission band.

Oligomeric conjugates based on butadyine bridges have also been synthesized, but emission quantum yields are typically lower due to larger structural flexibility, which promotes non-radiative deactivations [116]. For instance, the linear array **38** schematized in Fig. 20 exhibits fluorescence at 830 nm with photoluminescence quantum yield of 0.08 [117, 118]. These longer systems allow the preparation of a variety of beautiful open and closed Zn-porphyrin nanorings **39**, by means of templated syntheses based on hexaphenylbenzene **40** equipped with terminal pyridine centers that bind the Zn ions [116, 119, 120] (Fig. 20). As a consequence of the bending of the π-conjugated system and of the intrinsic high symmetry, such nanorings **39** exhibit uniquely broad NIR emission bands extending between 800 and over 1200 nm, which are strongly affected also by the presence/absence of the templating unit. However, emission quantum yields are below 1 % [118].

3.6 Phthalocyanines

Phthalocyanines are analogues of tetrabenzoporphyrins bearing N atoms in the ring *meso* position instead of C atoms (Fig. 7); accordingly, they are also termed tetrabenzotetraazaporphyrins. Similarly to porphyrins, they are characterized by two groups of absorption bands in the UV–Vis region, but their position, separation, and intensity is substantially different. The B band, corresponding to the $S_0 \rightarrow S_2$

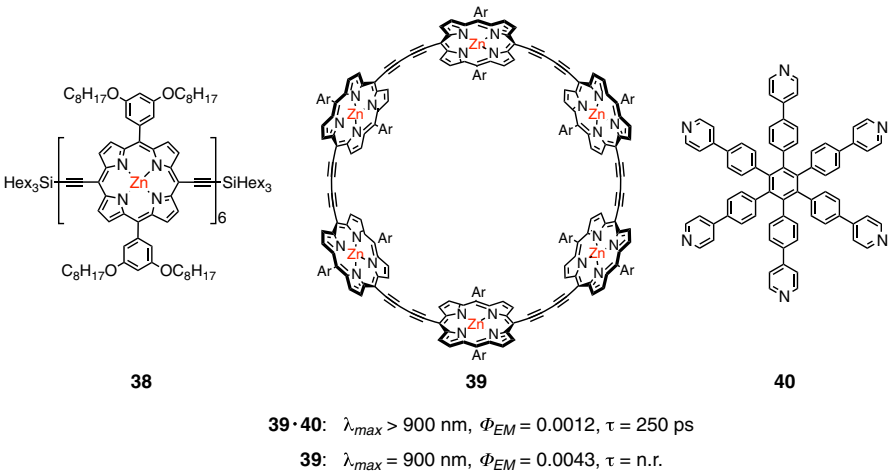

Fig. 20 Linear **38** and nanoring Zn-porphyrin hexameric arrays **39** connected through butadyine bridges. Both exhibit NIR emission in toluene (1 % pyridine), but the unique structural properties of the nanoring favors the lowering of the excited state energy and the luminescence quantum yield drops below 1 %. *Right* the hexadentate template **40** used for the synthesis of the nanoring

transition, is placed at about 350 nm, whereas the Q band—red-shifted and substantially increased in intensity—is located in the region between 600 and 700 nm [121]. The strong absorption in the red spectral region makes phthalocyanines widely utilized green–blue dyes and excellent candidates as photosensitizers for solar cells [122], photodynamic therapy agents [123], and several other applications [121]. Phthalocyanines can host a wide number of metal ions in the core and may undergo extensive chemical functionalization. This affords a remarkable tuning of the optical properties as a function of the nature of the central metal, the nature and position of the peripheral substituents, the sequential addition of fused benzene rings, and the deviation from planarity that may ensue [121, 124].

As far as luminescence is concerned, phthalocyanines exhibit a π–π^* fluorescence band with typically very small Stokes' shift (100–200 cm^{-1}) relative to the Q-band absorption features, which is attributed to the strong rigidity of the macrocyclic ring [121]. Free base and Zn(II)-phthalocyanines are the most investigated systems, but only the former show emission maxima systematically above 700 nm and can be classified as NIR fluorophores, although some examples of NIR-emitting Zn(II)-phthalocyanines have been also reported [121, 125]. In Fig. 21 are depicted some examples of free base (**41**, **42**) and Zn(II)-phthalocyanines (**43**, **44**), which are strongly emitting in the NIR region in THF solution. Electron-withdrawing and electron-donating substituents for free base and, respectively, Zn(II)-phthalocyanines have been used to enhance the emission output [125]. However, rationale emission tuning criteria cannot be drawn, because a clear correlation between the electronic features of the substituents and the fluorescence quantum yield has not been established [121].

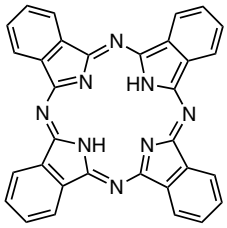

41

λ_{max} = 705 nm, Φ_{EM} = 0.60, τ = 6.9 ns

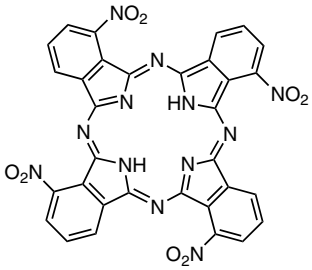

42

λ_{max} = 702 nm, Φ_{EM} = 0.79, τ = 7.4 ns

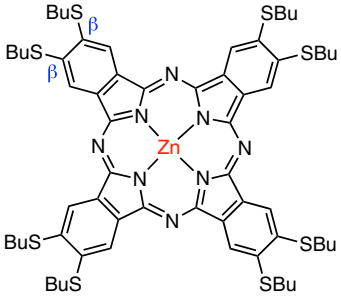

43

λ_{max} = 733 nm, Φ_{EM} = 0.12, τ = 3.2 ns

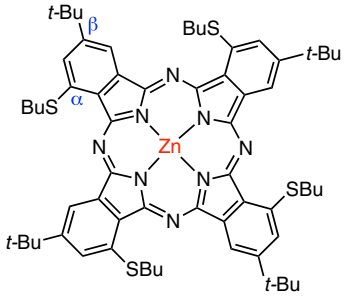

44

λ_{max} = 727 nm, Φ_{EM} = 0.22, τ = 3.1 ns

Fig. 21 Selected examples of strongly emitting free base and Zn(II)-phthalocyanines in THF solution [125]. Very few other examples with similar performance can be found in Ref. [121]

Several phthalocyanines of heavy metal ions—Rh(III), Pd(II), Ir(III), Pt(II)—exhibit phosphorescence in solution at room temperature between 950 and 1100 nm [121, 126], often in combination with fluorescence between 700 and 730 nm [127]. However, both emission quantum yields are rather low (<1 %) even in the best cases of Pt(II) and Pd(II) phthalocyanines [121, 127]. Also naphthalocyanines of the same heavy metals listed above exhibit fluorescence and phosphorescence quantum yields below 1 %, with triplet emission at $\lambda > 1230$ nm and down to 1340 nm for Pd(II)-based systems [128].

An interesting alternative to tetrabenzoporphyrins and phthalocyanines has been proposed by Borisov et al., who were able to synthesize "intermediate" azatetrabenzoporphyrin structures with both C and N atoms in the *meso* positions of the ring and then make Pt(II) **45** and Pd(II) **46** complexes [129]. These compounds exhibit remarkable phosphorescence in the NIR at room temperature in toluene, lower than Pt(II) and Pd(II) *meso*-tetraphenyltetrabenzoporphyrins (**18**, Fig. 10), but much stronger than related phthalocyanines. The strongest emitters of the series are reported in Fig. 22.

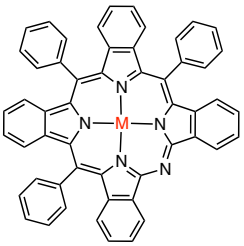

45 M = Pt: λ_{max} = 844 nm, Φ_{EM} = 0.40, τ = 22 µs

46 M = Pd: λ_{max} = 875 nm, Φ_{EM} = 0.08, τ = 213 µs

Fig. 22 The strongest emitting Pt(II)- and Pd(II)-azatetrabenzoporphyrin reported by Borisov et al. [129]. Photophysical data are in oxygen-free toluene at 298 K

4 Transition Metal Complexes

Phosphorescent transition metal complexes are a versatile class of emitters and offer several important advantages over traditional fluorescent materials. For instance: the $T_1 \rightarrow S_0$ phosphorescence enables the harvesting of both singlet and triplet excitons in electroluminescent devices (OLEDs, LECs) to achieve the maximum internal quantum efficiency; they exhibit large Stokes' shifts because of the $S_1 \rightarrow T_1$ intersystem crossing, induced by the relatively large spin–orbit coupling of the transition metal center; the emissive excited state has long lifetime, ranging from µs to ms. The most common excited states of phosphorescent transition metal complexes have a charge transfer nature, including metal-to-ligand (MLCT), ligand-to-ligand (LLCT), intraligand (ILCT), metal–metal-to-ligand (MMLCT) charge transfer. The most effective way for tuning the phosphorescence of transition metal complexes involves the modification of the ligands. Several design factors, such as changing the π-conjugation length, altering the substituents, e.g., by including donor–acceptor push–pull systems, or adding heterocycles, can be considered. In the case of multinuclear complexes also the effect of intramolecular metal–metal interactions, leading to red-shifted emission from ^{3}MMLCT excited states, should be taken into account. Intermolecular interactions, such as hydrogen bonding, π–π stacking, or charge transfer can be present in condensed phase. These can lead to the formation of excimers, exciplexes, or aggregates that can result in red-shifted emission. Up to now, there have appeared only a few reviews on the NIR phosphorescence of transition metal complexes [9, 130, 131].

4.1 Complexes of d^6 Metal Centers

4.1.1 Re(I)

Re(I) complexes of the type $[Re(N\hat{}N)(CO)_3L]^{n+}$ (where N^N = diimine ligand, L monodentate ligand, and $n = 0, 1$) exhibit room temperature (RT) phosphorescence and have been widely investigated [132, 133]. They usually display a structureless red emission at about 600 nm with small quantum yields ($<10^{-3}$) typically from ^{3}MLCT excited states. The emission band can be tuned by introducing electron-withdrawing or -donating groups on the diimine ligand. Using this strategy,

complexes with emission bands close to 800 nm have been prepared by Meyer and coworkers [134–136]. The introduction of the acetylide as the monodentate ligand into the d^6 metal diimine system raises the energy of the metal centered d–d states. This improves the population of the ^{3}MLCT state and induces a red shift of the transition energies, as demonstrated by the research group of Yam [137]. Strong emitting rhenium tricarbonyl complexes have been prepared by Rillema and coworkers using phenanthroline derivatives and 2,6-dimethylphenylisocyanide ligands [138, 139]. These represent the Re(I) complexes with the highest quantum yield prepared so far ($\Phi_{EM} = 0.83$ and $\tau = 20.2$ μs). However, the emission wavelength is significantly blue shifted ($\lambda_{max} = 510$ nm). More recently, a series of deep-red to NIR-emitting Re(I) complexes **47a–e** with good quantum yield ($\lambda_{max} = 680$–710 nm and $\Phi_{EM} = 0.01$–0.07 in CH_2Cl_2 solution at RT) have been prepared by Yam and coworkers [140]. Here, the metal center was coordinated by a bipyridine moiety inserted into a D–π–A–π–D structure (Fig. 23). The observed luminescence has been attributed to an intraligand charge transfer (^{3}ILCT) from the

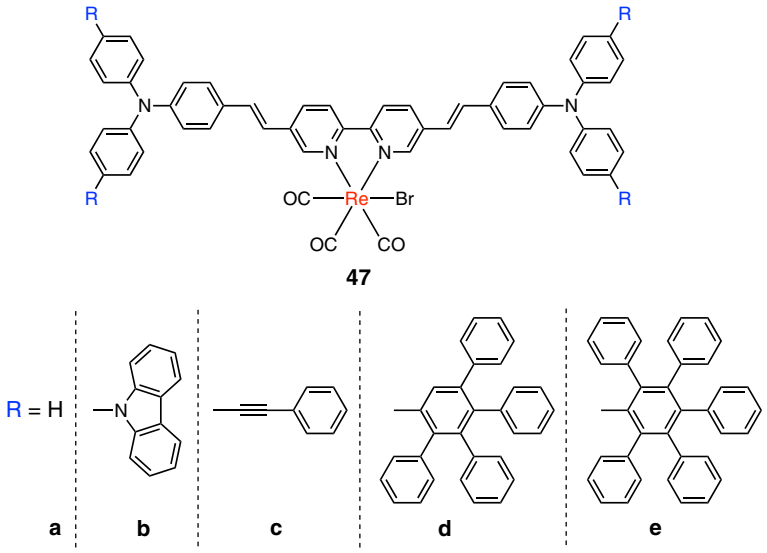

47a: $\lambda_{max} = 680$ nm, $\Phi_{EM} = 0.06$, $\tau < 0.1$ μs

47b: $\lambda_{max} = 701$ nm, $\Phi_{EM} = 0.01$, $\tau < 0.1$ μs

47c: $\lambda_{max} = 686$ nm, $\Phi_{EM} = 0.04$, $\tau = 0.11$ μs

47d: $\lambda_{max} = 703$ nm, $\Phi_{EM} = 0.06$, $\tau < 0.1$ μs

47e: $\lambda_{max} = 708$ nm, $\Phi_{EM} = 0.07$, $\tau < 0.1$ μs

Fig. 23 Chemical structures of some of the best-performing NIR-emitting Re(I) complexes [140]. Photophysical data are in CH_2Cl_2 at 298 K

triarylamine to the bipyridine. To the best of our knowledge, these are the brightest NIR-emitting Re(I) complexes reported in the literature.

4.1.2 Os(II) and Ru(II)

Polypyridine complexes of Os(II) and Ru(II) have similar photophysical behavior with emissive excited states of ^{3}MLCT character and an octahedral coordination geometry [141–145]. The energy of Os(II) luminescence is lower with respect to that of the Ru(II) analogues, because of the significantly more negative oxidation potential of the Os metal center [143, 144]. Although Os(II) complexes with high quantum yield in the visible region have been reported [143, 146], the luminescence quantum yield quickly drops below 10^{-2} in the NIR. This is due to the so-called "energy gap law" [7, 147], which forecasts an exponential increase of the non-radiative deactivation rate constant as the energy gap between the excited emitting state and the ground state decreases:

$$k_{\mathrm{nr}} = \alpha e^{-\beta \Delta E}.$$

Moreover, the excited state lifetime of Os(II) complexes is shorter than that of the Ru(II) homologues, because of the stronger spin–orbit coupling (SOC) in the former, which facilitates the intersystem crossing (ISC) from the triplet excited state to the singlet ground state. The emission of Os(II) complexes can be shifted in the NIR by using diimine ligands with electron-withdrawing substituents or with extended π-conjugation. Notably, using the latter strategy, weak emission bands maximizing up to 1270 nm has been reported by Kol and coworkers ($\Phi_{\mathrm{EM}} < 10^{-4}$ and $\tau < 4$ ns) for a series of $[\mathrm{Os(eilatin)}]^{2+}$ derivatives **48a–c** (Fig. 24) [148–150].

Recently, Wu and coworkers prepared a series of neutral Os(II) complexes **49a–d** (Fig. 25) using two isoquinolyl triazolate chromophores and ancillary phosphine ligands both in *trans* and *cis* arrangement [151]. These complexes exhibit a strong deep-red and NIR phosphorescence emission ($\lambda_{\max} = 602$–805 nm, $\Phi_{\mathrm{EM}} = 0.04$–$0.15$ and $\tau = 0.16$–0.76 μs) of MLCT character mixed with more localized ligand centered ILCT/LLCT transitions (Fig. 25). This series of charge-neutral and volatile Os(II) complexes, make them ideal for the fabrication of NIR-emitting OLED via thermal vacuum deposition.

The photochemistry and photophysics of Ru(II) polypyridyl complexes is mainly dominated by emitting excited states with MLCT character, suffering from the presence of close-lying d–d metal centered (MC) excited states that can lead to photosubstitution reactions and subsequent non-radiative deactivation [141, 142]. The spin–orbit coupling induced by the heavy metal atom causes large singlet–triplet mixing and, accordingly, these excited states usually possess triplet multiplicity. Several strategies have been applied to shift the emission of Ru(II) complexes into the NIR. Beside the polypyridyl ligand modifications mentioned above for the Os(II) complexes, which lower the energy of the LUMO, the destabilization of the metal t_{2g} orbitals with strong σ-donating ligands proved to be particularly effective [152]. This has been accomplished, for instance, with monodentate isothiocyanates –NCS **50** or cyclometalating ligands **51** (Fig. 26)

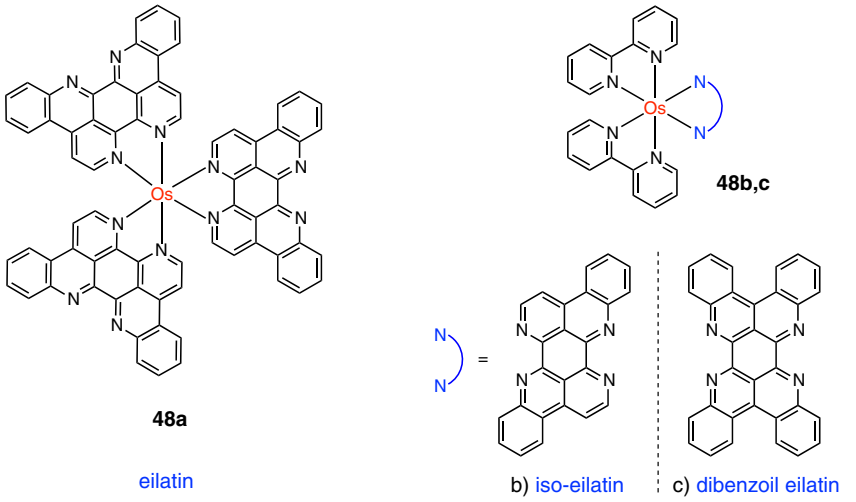

48a: λ_{max} = 1087 nm, Φ_{EM} = 1.4x10^{-4}, τ = n.r.

48b: λ_{max} = 1240 nm, Φ_{EM} <10^{-6}, τ < 0.1 µs

48c: λ_{max} = 1132 nm, Φ_{EM} = 6x10^{-5}, τ = 4 ns

Fig. 24 Chemical structures of some of NIR-emitting Os(II) complexes featuring fused aromatic ligands with extended π-conjugation [148–150]. Photophysical data are in CH_3CN at 298 K

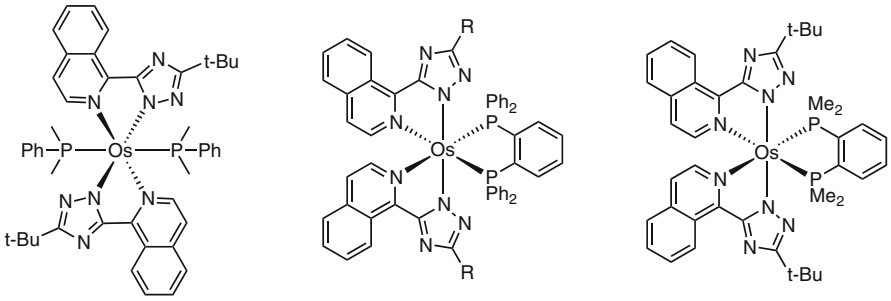

49a: λ_{max} = 805 nm, Φ_{EM} = 0.002, τ = 0.04 µs

49b: λ_{max} = 602 nm, Φ_{EM} = 0.15, τ = 0.76 µs

49c: λ_{max} = 695 nm, Φ_{EM} = 0.08, τ = 68 µs

49d: λ_{max} = 731 nm, Φ_{EM} = 0.04, τ = 0.16 µs

Fig. 25 Chemical structure of neutral charged NIR-emitting Os(II) complexes [151]. Photophysical data are in CH_2Cl_2 at 298 K

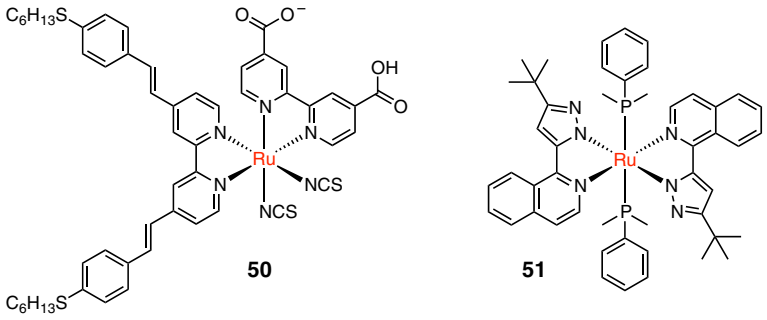

Fig. 26 Chemical structures of NIR-emitting Ru(II) complex with bidentate ligands [153, 155]

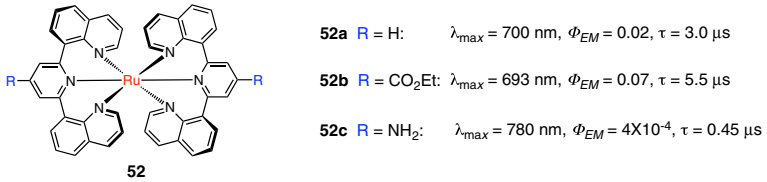

Fig. 27 Chemical structures of NIR-emitting Ru(II) complex with bis-terdentate ligands [156, 157]. Photophysical data are in MeOH:EtOH solution at 298 K

[153]. As for the osmium congener, the quantum yield rapidly drops for ruthenium complexes emitting in the NIR (typically, $\Phi_{EM} < 10^{-3}$ for $\lambda_{max} > 700$ nm) [9]. An alternative strategy involves the coordination of the strong electron donor quinonoid organometallic linker [Cp*Ru($C_6H_4O_2$)] with a low-lying π-acceptor polypyridyl ligand. This enables the tuning of the HOMO–LUMO gap, inducing a bathochromic shift of the MLCT transition up to 950–970 nm, but still with low quantum yields ($\Phi_{EM} < 0.002$) [154]. The concomitant use of two cyclometalating isoquinolyl-pyrazolate ligands arranged in *cis* configuration, together with two phosphinic monodentate ligands in the axial positions to complete the octahedral coordination sphere (**51**, Fig. 26), yield the brightest Ru(II) NIR-emitting complex with bidentate ligands reported so far in the literature ($\lambda_{max} = 709$ nm, $\Phi_{EM} = 0.02$ in the solid state) [155].

Terpyridine-like ligands offer several advantages over bidentate ligands; for instance, they afford achiral complexes which can undergo easy linear extension. Furthermore, cyclometalated terdentate ligands typically show higher stability and a red-shifted emission with respect to the parent tris-bipyridyne complexes. Typically, these features are accompanied by a lower luminescence quantum yield because of the poorer bite angles and weaker ligand field strengths of polypyridine terdentate ligands [142]. Again, the presence of electron-withdrawing or -donating groups induces a bathochromic shift of the emission into the NIR region, while the presence of electron-withdrawing substituents improve the luminescence quantum yields and lifetime. In particular, the bis-terdentate complexes **52a–c** depicted in Fig. 27

display the best NIR emission features reported among the Ru(II) complexes ($\lambda_{max} \sim 700$ nm, $\Phi_{EM} = 0.07$ and $\tau = 5.5$ μs) [156, 157].

4.1.3 Ir(III)

Mononuclear Ir(III) complexes are the most efficient and versatile class of phosphorescent emitters. The strong spin–orbit coupling of the Ir atom ($\zeta_{Ir} = 3909$ cm^{-1} [158]) induces a mixing of singlet and triplet states, mainly of MLCT or ILCT character. In the case of cyclometalated complexes, the usual assumption used to interpret the spectroscopic properties of inorganic complexes, i.e., that both the ground and excited states can be described by a localized molecular orbital (MO) configuration, is less applicable. The large degree of covalency in the Ir–C σ bonds might promote transitions with σ bond to ligand charge transfer (SBLCT) or mixed MLCT/intraligand charge transfer (ILCT) character. The outstanding luminescence properties can be tuned so as to cover a full range of visible colors, from blue to red. Extension into the NIR can be achieved upon judicious modification of the ligands [159].

It has been demonstrated that the increase of the extension of π-conjugation in the cyclometalating ligand is the most effective way to red-shift the emission energy, while the effect of substituents has typically a more limited influence [159–161]. Using this strategy, a series of Ir(III) complexes with bidentate ligands (**53a–e**, Fig. 28) which display emission maxima above 900 nm and $\Phi_{EM} < 0.02$ have been prepared by Chen et al. [162]. The use of terdentate cyclometalating

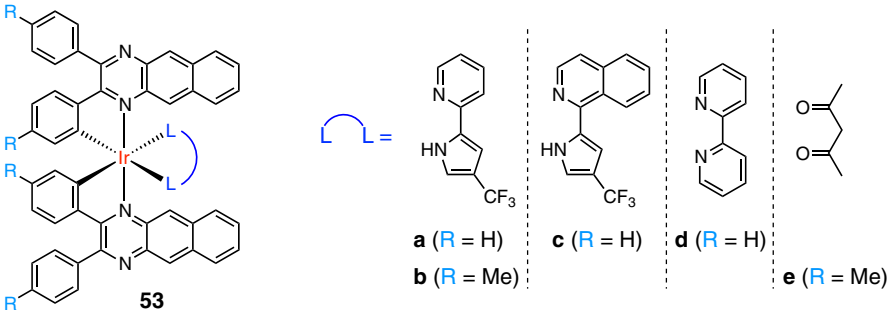

53a: $\lambda_{max} = 916$ nm, $\Phi_{EM} = 6.5 \times 10^{-3}$, $\tau = 286$ ns

53b: $\lambda_{max} = 916$ nm, $\Phi_{EM} = 0.01$, $\tau = 302$ ns

53c: $\lambda_{max} = 922$ nm, $\Phi_{EM} = 9.5 \times 10^{-3}$, $\tau = 276$ ns

53d: $\lambda_{max} = 922$ nm, $\Phi_{EM} = 3.6 \times 10^{-3}$, $\tau = 403$ ns

53e: $\lambda_{max} = 904$ nm, $\Phi_{EM} = 0.022$, $\tau = 290$ ns

Fig. 28 Chemical structures of NIR-emitting Ir(III) complexes featuring cyclometalating ligands with extended π-conjugation [162]. Photophysical data are in CH_2Cl_2 solution at 298 K

ligands of the type C^N^C or C^C^N proved to be effective in the preparation of far-red emitting phosphors with moderate quantum yield (ca. 0.03) but with emission wavelength below 700 nm (ca. 680 nm) and thus these cannot be considered as pure NIR emitters [163]. The latter, based on mononuclear Ir(III) complexes are rare, and the few examples reported in the literature show low emission quantum yields, around 10^{-3}–10^{-4}, with $\lambda_{max} > 700$ nm. However, it must be noted that most efforts have been devoted to the preparation of strong emitting visible phosphors for optoelectronic application.

4.2 Complexes of d^8 Metal Centers

4.2.1 Pt(II) and Au(III)

d^8 metal ions preferentially form four-coordinate square planar complexes in the presence of strong-field ligands. This geometry may enable Pt–Pt interactions and is responsible for many of the key features that characterize the absorption, luminescence and other excited state properties of Pt(II) complexes [164]. As for other transition metal complexes, the high SOC of the metal center induces an efficient singlet–triplet intersystem crossing. Therefore, the resulting emission is mainly phosphorescence. The presence of a strong ligand field enhances the luminescence in solution because of the destabilization of the MC excited states that can drain the excitation energy through non-radiative pathways.

In Pt(II) complexes with polyimine bidentate ligands, the introduction of π-extended systems on the acetylide ligands **54** or the use of strongly π-accepting ligands (Fig. 29) have proved to be efficient methods to shift the emission energy

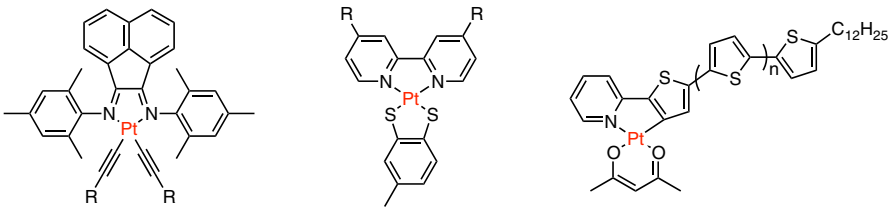

54

55a: R = Cl
55b: R = COOEt

56a: n = 1
56b: n = 2

54 : λ_{max} = 786-896 nm, Φ_{EM} = 5.3-9x10^{-5}, τ = 36-8 ns

55a: λ_{max} = 738 nm, Φ_{EM} = 4.3x10^{-5}, τ = 157 ns

55b: λ_{max} = 785 nm, Φ_{EM} = 0.4x10^{-5}, τ = 68 ns

56a: λ_{max} = 706 nm, Φ_{EM} = 0.058, τ = 2.3 μs

56b: λ_{max} = 735 nm, Φ_{EM} = 0.020, τ = n.r.

Fig. 29 Selected examples of NIR-emitting Pt(II) complexes with bidentate ligands [165–168]. Photophysical data are in CH_2Cl_2 solution at 298 K

into the NIR, up to 900 nm, but still with small luminescence quantum yields ($\Phi_{EM} < 0.01$) [165]. Other types of bidentate ligands as, for instance, dithiolates **55a–b** [166, 167], and cyclometalating (thiophenyl)pyridines **56a–b** bearing extended conjugated systems [168] have been used to prepare NIR-emitting Pt(II) complexes (Fig. 29).

The prototype complex with terdentate ligand terpyridine (tpy) $[Pt(tpy)Cl]^+$ is known to be non emissive in solution due to the presence of low-lying MC excited states that effectively quench the luminescence from ^{3}MLCT states. However, modification of the tpy ligand and/or substitution of the halide moiety with strong field ligands, such as alkynyls (**57**, Fig. 30), can improve the photophysical properties of these complexes [164]. The presence of the terdentate ligand inhibits the distortion exhibited by bis-bidentate complexes, because of the twisting of the two planes in the excited state. As a consequence, in Pt(II) square planar complexes with terdentate ligands the metal center is more prone to undergo Pt–Pt interactions, especially in condensed phases. Thus, on going from the solution to the solid state, the nature of the lowest energy emission band switches from ^{3}MLCT to ^{3}MMLCT and its energy is also red-shifted (λ_{max} = 710–800 nm) [169]. A similar effect can be obtained with N^N^N ligands involving π-extended systems (**58** and **59**, Fig. 30), which are able to emit in the NIR in dilute solution with moderate quantum yields (**58**: λ_{max} = 700 nm, Φ_{EM} = 0.03) [170].

By incorporating a cyclometalating ring into a terdentate ligand, the luminescence efficiency can be further increased and ^{3}MMLCT NIR excimeric luminescence has been observed with C^N^N ligands (λ_{max} = 700 nm, Φ_{EM} = 0.03) (**60**, Fig. 31) [172]. Similar behavior is displayed by the parent Pt(II) complexes with N^C^N ligands **61a–c** (Fig. 31), with NIR emission at 700 nm in aggregated states, but with greatly enhanced intensity (Φ_{EM} = 0.24–0.35) [173]. The introduction of trifluoromethyl groups onto the N^C^N ligand (**62a–c**, Fig. 31) induces a further red-shift in the excimer emission (λ_{max} = 734 nm) [174]. To the best of our

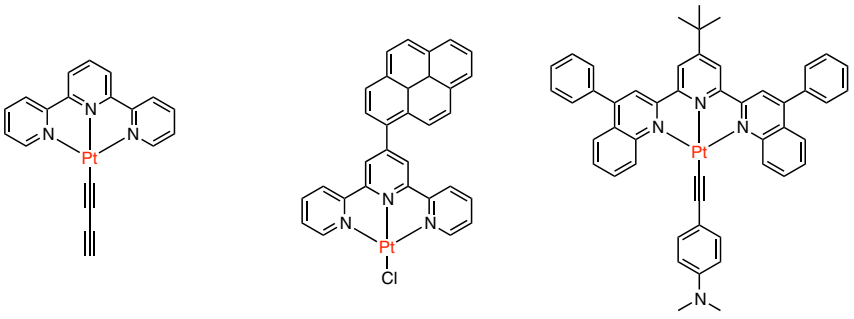

57 **58** **59**

λ_{max} = 670 nm, Φ_{EM} = 0.011
τ = 785 μs

λ_{max} = 700 nm, Φ_{EM} = 0.034
τ = 64 μs

λ_{max} = 686 nm, Φ_{EM} = 0.11
τ = 2.4 μs

Fig. 30 Selected examples of NIR-emitting Pt(II) complexes with polypyridine terdentate ligands [169–171]. Photophysical data are in CH_3CN (**57**) and CH_2Cl_2 (**58** and **59**) at 298 K

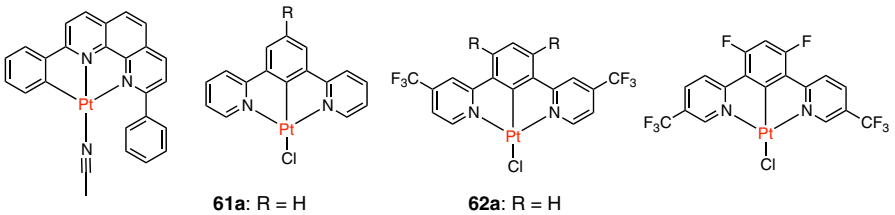

60 **61a**: R = H **61b**: R = CH_3 **61c**: R = COOMe **62a**: R = H **62b**: R = F **62c**

60: λ_{max} = 700 nm, Φ_{EM} = 0.032, τ = 0.9 μs

61a: λ_{max} = 700 nm, Φ_{EM} = 0.24, τ = 0.98 μs

61b: λ_{max} = 700 nm, Φ_{EM} = 0.31, τ = 1.10 μs

61c: λ_{max} = 700 nm, Φ_{EM} = 0.35, τ =1.04 μs

62a: λ_{max} = 756 nm

62b: λ_{max} = 734 nm

62c: λ_{max} = 717 nm

Fig. 31 Selected examples of NIR emission from excimeric states in Pt(II) complexes with terdentate cyclometalating ligands [172–174]. Photophysical data are in CH_2Cl_2 (**60**) and neat solid film (**61a–c, 62a–c**) at 298 K

knowledge, the latter value is the record among NIR-emitting transition metal complexes.

The study of the photophysics of Au(III) cyclometalated complexes has mainly focused on terdentate C^N^N and C^N^C type ligands [175]. The presence of low-lying metal centered (MC) and ligand to metal charge transfer (LMCT) excited states quenches the luminescence from the ligand centered (LC) excited levels. As for the d^{10} Au(I) analogues, the incorporation of strong σ donating auxiliary ligands is a successful way to enhance the photophysical performances of this class of complexes ($\Phi_{EM} > 0.1$). However, the examples reported in the literature display emission in the visible range ($\lambda_{max} = 520$ nm) [176].

4.3 Complexes of d^{10} Metal Centers

4.3.1 Au(I) and Cu(I)

The most common coordination geometries displayed by d^{10} Au(I) complexes are linear or trigonal planar. The luminescence observed in mononuclear Au(I) complexes mainly originates from ^{3}LMCT or ^{3}LLCT excited states [175]. NIR-emitting mononuclear Au(I) complexes are very rare and with faint luminescence [9]. In polynuclear gold complexes, the presence of intra- or intermolecular Au–Au interactions lowers the energy of the lowest excited state and a NIR emission can be observed. In this case, the phosphorescence can arise from ligand-to-metal–metal charge transfer (LMMCT) excited states. However, NIR-emitting polynuclear clusters usually show a weak luminescence ($\Phi_{EM} < 10^{-3}$) in the range 700–900 nm [177].

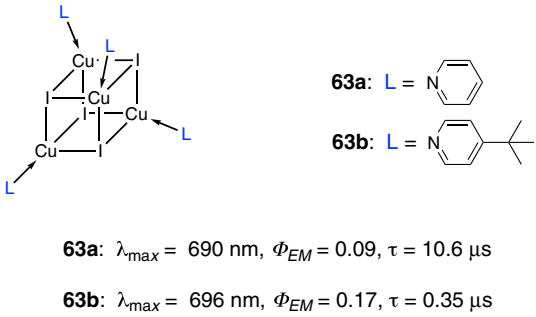

Fig. 32 Chemical structures of the best performing NIR-emitting $[Cu_4X_4L_4]$ type clusters [183]. Photophysical data are in toluene solution at 298 K

Cu(I) complexes adopt a tetrahedral coordination of the ligands to the metal center which usually undergoes a strong Jahn–Teller flattening in the excited state. The consequent formation of a five-coordinated square pyramidal exciplex promotes non-radiative decay patterns. For this reason, $[Cu(N\hat{}N)_2]^+$ or $[Cu(N\hat{}N)(P\hat{}P)]^+$ complexes display only weak NIR phosphorescence ($\lambda_{max} > 700$ nm, $\Phi_{EM} < 10^{-3}$) from ^{3}MLCT excited states [178, 179]. Cu_4I_4 and Cu_6S_6 clusters and halogenido bridged dimers Cu_2X_2 have been extensively studied for their remarkable luminescence performance that stems from Cu to Cu interactions [180–182]. There are several examples of $[CuX_4L_4]$ (where X = Br, I and L is a monodentate ligand, usually a pyridine derivative) NIR-emitting clusters with cubane-like geometry. Among them, those reported by Ford and coworkers (**63a–b**, Fig. 32) display the highest quantum yield reported so far in the NIR region for this class of compounds (Φ_{EM} = 0.03–0.17 and τ = 0.11–44.2 μs) [183].

5 Conclusions

We have examined three classes of NIR luminescent systems (i.e., with emission maximum above 700 nm) that have emerged in recent years; the photophysical data of all the molecules and metal complexes that have been discussed are gathered in the Table 1 (λ_{EM}, Φ_{EM}, τ). Our overview starts with organic dyes and includes cyanines, pyrrolopyrrole cyanines, squaraines, BODIPYs, rhodamines and donor–acceptor chromophores. Successful strategies adopted to push the emission characteristics of the organic dyes into the NIR region include extension of π-conjugation, stiffening the chromophore π-backbone by chelation, introduction of σ*–π* conjugation, and linking electron donor and acceptor molecular units through a conjugated π-spacer. Second, we have examined the vast family of porphyrinoids, which entails several core structures such as porphyrins (standard, extended, fused, ring-shaped), bacteriochlorins, and phthalocyanines. These are a highly versatile class of NIR luminophores that can tune the emission character from fluorescence to phosphorescence by metal complexation, may exhibit emission all the way from 700 to beyond 1200 nm and can show respectable photoluminescence quantum yields (>10 %) even above 1000 nm.

Table 1 Photophysical data of all the NIR infrared emitters presented in this paper

Compound	Solvent	λ_{max}, nm	Φ_{EM}	τ	Refs.
1a	H_2O	803	0.17		[23]
1b	H_2O	757	0.47		[23]
2	CH_2Cl_2	915			[26]
3a	$CHCl_3$	708–805	0.32–0.69		[28]
3b	$CHCl_3$	749–881	0.32–0.62		[28]
4a	$CHCl_3$	867			[29]
4b	$CHCl_3$	966			[29]
5a	CH_2Cl_2	698	0.37		[40, 41]
5b	CH_2Cl_2	708	0.47		[40, 41]
5c	CH_2Cl_2	710	0.47		[40, 41]
5d	CH_2Cl_2	713	0.58		[40, 41]
6a	CH_2Cl_2	890	0.10		[40, 41]
6b	CH_2Cl_2	913	0.11		[40, 41]
6c	CH_2Cl_2	916	0.12		[40, 41]
6d	CH_2Cl_2	922	0.17		[40, 41]
7	H_2O pH = 7.4	712	0.12		[54]
8	Ethanol	721–763	0.29–0.56		[55]
9a	Toluene	1065	0.071		[56]
9b	Toluene	1120	0.028		[56]
9c	Toluene	1230	0.018		[56]
10a	Toluene	1055	0.185		[56]
10b	Toluene	1120	0.046		[56]
10c	Toluene	1285	0.019		[56]
11a	Toluene	1125	0.053		[56]
11b	Toluene	1295	0.011		[56]
11c	Toluene	1360	<0.01		[56]
12	Toluene	726	0.001	30 μs	[75, 76]
13	Toluene	760	0.3	23 μs	[78]
14	CH_2Cl_2	866	0.06	21 μs	[81]
15	Toluene	770	0.49	53 μs	[84]
16	Toluene	891	0.15	12.7 μs	[84]
17	Toluene	1022	0.08	3.2 μs	[84]
18	Toluene	773	0.35	30 μs	[85, 86]
	2-Me-THF	765	0.70	53 μs	
19	Toluene	803	0.23	297 μs	[88]
20	CH_2Cl_2	705	0.06		[96]
21	CH_2Cl_2	741	0.10		[93]
22	CH_2Cl_2	900	0.003		[97]
23a	Toluene	716	0.14	4.0 ns	[101]
23b	Toluene	725	0.10	3.4 ns	[101]
24a	Toluene	805	0.15	3.2 ns	[101]
24b	Toluene	825	0.17	3.6 ns	[101]

Table 1 continued

Compound	Solvent	λ_{max}, nm	Φ_{EM}	τ	Refs.
25	Toluene	759	0.19	5.7 ns	[102]
28	Toluene	1080	3.5×10^{-4}	5.7 ns	[106]
29	Toluene	736	0.10	1.4 ns	[109]
30	Toluene	960	0.017	0.25 ns	[109]
32	CH_2Cl_2	721	0.08	1.5 ns	[110]
33	CH_2Cl_2	829	0.08	0.25 ns	[110]
34	CH_2Cl_2	839	0.13	0.25 ns	[110]
35a	Toluene	953		0.8 ns	[114]
	THF	1050		0.4 ns	
35b	Toluene	956		0.7 ns	[114]
	THF	1040		0.3 ns	
35c	Toluene	945		1.1 ns	[114]
	THF	1053		0.4 ns	
36	THF	806	0.22	1.13 ns	[115]
37	THF	883	0.14	0.45 ns	[115]
39	Toluene	900	0.0043		[118]
39•40	Toluene	>900	0.0012	250 ps	[118]
41	THF	705	0.60	6.9 ns	[125]
42	THF	702	0.79	7.4 ns	[125]
43	THF	733	0.12	3.2 ns	[125]
44	THF	727	0.22	3.1 ns	[125]
45	Toluene	844	0.40	22 μs	[129]
46	Toluene	875	0.08	213 μs	[129]
47a	CH_2Cl_2	680	0.06	<0.1 μs	[140]
47b	CH_2Cl_2	701	0.01	<0.1 μs	[140]
47c	CH_2Cl_2	686	0.04	0.11 μs	[140]
47d	CH_2Cl_2	703	0.06	<0.1 μs	[140]
47e	CH_2Cl_2	708	0.07	<0.1 μs	[140]
48a	CH_3CN	1087	1.4×10^{-4}		[148]
48b	CH_3CN	1240	$<10^{-6}$	<0.1 μs	[149]
48c	CH_3CN	1132	6×10^{-5}	0.004 μs	[150]
49a	CH_2Cl_2	805	0.002	0.04 μs	[151]
49b	CH_2Cl_2	602	0.15	0.76 μs	[151]
49c	CH_2Cl_2	695	0.08	0.68 μs	[151]
49d	CH_2Cl_2	731	0.04	0.16 μs	[151]
50	DMF	780			[153]
51	CH_2Cl_2	718			[155]
52a	MeOH:EtOH	700	0.02	3.0 μs	[156, 157]
52b	MeOH:EtOH	693	0.07	5.5 μs	[156, 157]
52c	MeOH:EtOH	780	4×10^{-4}	0.45 μs	[156, 157]
53a	CH_2Cl_2	916	0.0065	0.286 μs	[162]
53b	CH_2Cl_2	916	0.01	0.302 μs	[162]

Table 1 continued

Compound	Solvent	λ_{max}, nm	Φ_{EM}	τ	Refs.
53c	CH_2Cl_2	922	9.5×10^{-3}	0.276 μs	[162]
53d	CH_2Cl_2	922	3.6×10^{-3}	0.403 μs	[162]
53e	CH_2Cl_2	904	0.022	0.290 μs	[162]
54	CH_2Cl_2	786–896	$5.3–9.0 \times 10^{-5}$	0.036–0.008 μs	[165]
55a	CH_2Cl_2	775	4.3×10^{-5}	0.157 μs	[166, 168]
55b	CH_2Cl_2	795	0.4×10^{-5}	0.068 μs	[166, 168]
56a	CH_2Cl_2	706	0.058	2.3 μs	[167]
56b	CH_2Cl_2	735	0.020		[167]
57	CH_3CN	670	0.011	785 μs	[169]
58	CH_2Cl_2	700	0.034	64 μs	[170]
59	CH_2Cl_2	686	0.11	2.4 μs	[171]
60	CH_2Cl_2	700	0.032	0.9 μs	[172]
61a	neat film	700	0.24	0.98 μs	[173]
61b	neat film	700	0.31	1.10 μs	[173]
61c	neat film	700	0.35	1.07 μs	[173]
62a	neat film	756			[174]
62b	neat film	734			[174]
62c	neat film	717			[174]
63a	Toluene	690	0.09	10.6 μs	[183]
63b	Toluene	696	0.17	10.3 μs	[183]

Finally, we have focused on transition metal complexes, presenting a survey related to d^6, d^8, and d^{10} metal ions—Re(I), Os(II), Ru(II), Ir(III), Pt(II), Au(III), Au(I), Cu(I)—with emphasis on the strategies to shift the emission in the NIR region and to increase the luminescence efficiency. Typical strategies to rationally modify the ligand frameworks include the change of the π-conjugation length, the inclusion of donor–acceptor push–pull systems, or the addition of heterocycles.

Overall, the progress in the area of NIR-emitting molecules overviewed herein suggests that the availability of robust, cheap, and strong NIR luminophores will further expand in the years to come, possibly widening the range of technological applications.

Acknowledgments We thank CNR [Project PHEEL, CNR-CONICET joint project "Carbon Dioxide Reduction on Photocatalytic Nanomaterials", CNR-CNRS(L) joint project "Development of a Modular Integrated Device for Solar Energy Conversion", and Progetto Bandiera N-Chem]. V.K.P. thanks department of science and technology (DST-SERB), Government of India for a Young Scientist Fellowship.

References

1. Ronda CR (ed) (2008) Luminescence—from theory to applications. Wiley, Weinheim
2. Armaroli N, Balzani V (2011) Energy for a sustainable world. From the oil age to a sun powered future, Chap. 9. Wiley, Weinheim

3. Kitai A (ed) (2008) Luminescent materials and applications, Wiley series in materials for electronic and optoelectronic applications. Wiley, Chichester
4. Mason WT (ed) (1999) Fluorescent and luminescent probes for biological activity: a practical guide to technology for quantitative real-time analysis, biological techniques. Academic Press, San Diego
5. Mirasoli M, Guardigli M, Michelini E, Roda A (2014) J Pharm Biomed Anal 87:36–52
6. Lakowicz JR (2006) Principles of fluorescence spectroscopy. Springer, New York
7. Englman R, Jortner J (1970) Mol Phys 18:145–164
8. Guo ZQ, Park S, Yoon J, Shin I (2014) Chem Soc Rev 43:16–29
9. Xiang HF, Cheng JH, Ma XF, Zhou XG, Chruma JJ (2013) Chem Soc Rev 42:6128–6185
10. Yuan L, Lin W, Zheng K, He L, Huang W (2013) Chem Soc Rev 42:622–661
11. Bünzli J-CG, Eliseeva SV (2010) J Rare Earth 28:824–842
12. Jiao C, Wu J (2012) Synlett 171–184
13. Avlasevich Y, Li C, Müllen K (2010) J Mater Chem 20:3814–3826
14. Bachilo SM, Strano MS, Kittrell C, Hauge RH, Smalley RE, Weisman RB (2002) Science 298:2361–2366
15. Piao YM, Meany B, Powell LR, Valley N, Kwon H, Schatz GC, Wang YH (2013) Nat Chem 5:840–845
16. Wang R, Zhang F (2014) J Mater Chem B 2:2422–2443
17. Locritani M, Yu YX, Bergamini G, Baroncini M, Molloy JK, Korgel BA, Ceroni P (2014) J Phys Chem Lett 5:3325–3329
18. Pansare VJ, Hejazi S, Faenza WJ, Prud'homme RK (2012) Chem Mater 24:812–827
19. Qian G, Wang ZY (2010) Chem Asian J 5:1006–1029
20. Strekowski L (ed) (2008) Heterocyclic polymethine dyes—synthesis, properties and applications, topics in heterocyclic chemistry. Springer, Heidelberg
21. Wang ZY (2013) Near-infrared organic materials and emerging applications. CRC Press, FL
22. Yuan L, Lin W, Zheng K, He L, Huang W (2013) Chem Soc Rev 42:622–661
23. Peng X, Song F, Lu E, Wang Y, Zhou W, Fan J, Gao Y (2005) J Am Chem Soc 127:4170–4171
24. Chen X, Peng X, Cui A, Wang B, Wang L, Zhang R (2006) J Photochem Photobiol A 181:79–85
25. Shershov VE, Spitsyn MA, Kuznetsova VE, Timofeev EN, Ivashkina OA, Abramov IS, Nasedkina TV, Zasedatelev AS, Chudinov AV (2013) Dyes Pigm 97:353–360
26. Bouit P-A, Di Piazza E, Rigaut S, Le Guennic B, Aronica C, Toupet L, Andraud C, Maury O (2008) Org Lett 10:4159–4162
27. Fischer GM, Ehlers AP, Zumbusch A, Daltrozzo E (2007) Angew Chem Int Ed 46:3750–3753
28. Fischer GM, Isomäki-Krondahl M, Göttker-Schnetmann I, Daltrozzo E, Zumbusch A (2009) Chem Eur J 15:4857–4864
29. Fischer GM, Daltrozzo E, Zumbusch A (2011) Angew Chem Int Ed 50:1406–1409
30. Fischer GM, Jüngst C, Isomäki-Krondahl M, Gauss D, Möller HM, Daltrozzo E, Zumbusch A (2010) Chem Commun 46:5289–5291
31. Ajayaghosh A (2005) Acc Chem Res 38:449–459
32. Sreejith S, Carol P, Chithra P, Ajayaghosh A (2008) J Mater Chem 18:264–274
33. McEwen JJ, Wallace KJ (2009) Chem Commun 6339–6351
34. Gassensmith JJ, Baumes JM, Smith BD (2009) Chem Commun 6329–6338
35. Beverina L, Salice P (2010) Eur J Org Chem 2010:1207–1225
36. Avirah RR, Jayaram DT, Adarsh N, Ramaiah D (2012) Org Biomol Chem 10:911–920
37. Qin C, Wong W-Y, Han L (2013) Chem Asian J 8:1706–1719
38. Hu L, Yan Z, Xu H (2013) RSC Adv 3:7667–7676
39. Anees P, Sreejith S, Ajayaghosh A (2014) J Am Chem Soc 136:13233–13239
40. Mayerhöffer U, Fimmel B, Würthner F (2012) Angew Chem Int Ed 51:164–167
41. Mayerhöffer U, Gsänger M, Stolte M, Fimmel B, Würthner F (2013) Chem Eur J 19:218–232
42. Loudet A, Burgess K (2007) Chem Rev 107:4891–4932
43. Ulrich G, Ziessel R, Harriman A (2008) Angew Chem Int Ed 47:1184–1201
44. Descalzo AB, Xu H-J, Shen Z, Rurack K (2008) Ann NY Acad Sci 1130:164–171
45. Boens N, Leen V, Dehaen W (2012) Chem Soc Rev 41:1130–1172
46. Kamkaew A, Lim SH, Lee HB, Kiew LV, Chung LY, Burgess K (2013) Chem Soc Rev 42:77–88
47. Ni Y, Wu J (2014) Org Biomol Chem 12:3774–3791
48. Lu H, Mack J, Yang Y, Shen Z (2014) Chem Soc Rev 43:4778–4823
49. Zhang X, Yu H, Xiao Y (2011) J Org Chem 77:669–673
50. Poirel A, De Nicola A, Ziessel R (2012) Org Lett 14:5696–5699

51. Lavis LD, Raines RT (2008) ACS Chem Biol 3:142–155
52. Beija M, Afonso CAM, Martinho JMG (2009) Chem Soc Rev 38:2410–2433
53. Sun Y-Q, Liu J, Lv X, Liu Y, Zhao Y, Guo W (2012) Angew Chem Int Ed 51:7634–7636
54. Koide Y, Urano Y, Hanaoka K, Piao W, Kusakabe M, Saito N, Terai T, Okabe T, Nagano T (2012) J Am Chem Soc 134:5029–5031
55. Yuan L, Lin W, Yang Y, Chen H (2011) J Am Chem Soc 134:1200–1211
56. Qian G, Dai B, Luo M, Yu D, Zhan J, Zhang Z, Ma D, Wang ZY (2008) Chem Mater 20:6208–6216
57. Qian G, Wang ZY (2010) Can J Chem 88:192–201
58. Ellinger S, Graham KR, Shi P, Farley RT, Steckler TT, Brookins RN, Taranekar P, Mei J, Padilha LA, Ensley TR, Hu H, Webster S, Hagan DJ, Van Stryland EW, Schanze KS, Reynolds JR (2011) Chem Mater 23:3805–3817
59. Bürckstümmer H, Weissenstein A, Bialas D, Würthner F (2011) J Org Chem 76:2426–2432
60. Kadish KM, Smith KM, Guilard R (eds) (2000) The porphyrin handbook. Academic Press, San Diego
61. Flamigni L (2007) J Photochem Photobiol C 8:191–210
62. Babu SS, Bonifazi D (2014) ChemPlusChem 79:895–906
63. Armaroli N, Marconi G, Echegoyen L, Bourgeois JP, Diederich F (2000) Chem Eur J 6:1629–1645
64. D'Souza F, Ito O (2009) Chem Commun 4913–4928
65. Mohnani S, Bonifazi D (2010) Coord Chem Rev 254:2342–2362
66. Vogel E (1996) Pure Appl Chem 68:1355–1360
67. Hill JP, D'Souza F, Ariga K (2012) In: Steed JV, Gale PA (eds) Supramolecular chemistry: from molecules to nanomaterials. Wiley, Hoboken
68. Bhupathiraju NVSDK, Rizvi W, Batteas JD, Drain CM (2016) Org Biomol Chem 14:389–408
69. Gouterman M (1961) J Mol Spectrosc 6:138–163
70. Harriman A, Hosie RJ (1981) J Chem Soc Faraday Trans 2(77):1695–1702
71. Kalyanasundaram K (1992) Photochemistry of polypyridine and porphyrin complexes, vol 13. Academic Press, London
72. Harriman A (1982) J Chem Soc Faraday Trans 1(78):2727–2734
73. Armaroli N, Diederich F, Echegoyen L, Habicher T, Flamigni L, Marconi G, Nierengarten J-F (1999) New J Chem 23:77–83
74. Kalyanasundaram K (1992) Photochemistry of polypyridine and porphyrin complexes, vol 15. Academic Press, London
75. Scandola F, Chiorboli C, Prodi A, Iengo E, Alessio E (2006) Coord Chem Rev 250:1471–1496
76. Prodi A, Indelli MT, Kleverlaan CJ, Scandola F, Alessio E, Gianferrara T, Marzilli LG (1999) Chem Eur J 5:2668–2679
77. Ikonen M, Guez D, Marvaud V, Markovitsi D (1994) Chem Phys Lett 231:93–97
78. Koren K, Borisov SM, Saf R, Klimant I (2011) Eur J Inorg Chem 2011:1531–1534
79. Flamigni L, Gryko DT (2009) Chem Soc Rev 38:1635–1646
80. Sinha W, Ravotto L, Ceroni P, Kar S (2015) Dalton Trans 44:17767–17773
81. Ke X-S, Zhao H, Zou X, Ning Y, Cheng X, Su H, Zhang J-L (2015) J Am Chem Soc 137:10745–10752
82. Borisov SM, Papkovsky DB, Ponomarev GV, DeToma AS, Saf R, Klimant I (2009) J Photochem Photobiol A 206:87–92
83. Finikova OS, Cheprakov AV, Vinogradov SA (2005) J Org Chem 70:9562–9572
84. Sommer JR, Shelton AH, Parthasarathy A, Ghiviriga I, Reynolds JR, Schanze KS (2011) Chem Mater 23:5296–5304
85. Borek C, Hanson K, Djurovich PI, Thompson ME, Aznavour K, Bau R, Sun YR, Forrest SR, Brooks J, Michalski L, Brown J (2007) Angew Chem Int Ed 46:1109–1112
86. Currie MJ, Mapel JK, Heidel TD, Goffri S, Baldo MA (2008) Science 321:226–228
87. Niedermair F, Borisov SM, Zenkl G, Hofmann OT, Weber H, Saf R, Klimant I (2010) Inorg Chem 49:9333–9342
88. Borisov SM, Nuss G, Haas W, Saf R, Schmuck M, Klimant I (2009) J Photochem Photobiol A 201:128–135
89. Saito S, Osuka A (2011) Angew Chem Int Ed 50:4342–4373
90. D'Souza F (2015) Angew Chem Int Ed 54:4713–4714
91. Lim JM, Yoon ZS, Shin J-Y, Kim KS, Yoon M-C, Kim D (2009) Chem Commun 261–273
92. Yoon ZS, Kwon JH, Yoon M-C, Koh MK, Noh SB, Sessler JL, Lee JT, Seidel D, Aguilar A, Shimizu S, Suzuki M, Osuka A, Kim D (2006) J Am Chem Soc 128:14128–14134

93. Xie YS, Wei PC, Li X, Hong T, Zhang K, Furuta H (2013) J Am Chem Soc 135:19119–19122
94. Yoon ZS, Cho D-G, Kim KS, Sessler JL, Kim D (2008) J Am Chem Soc 130:6930–6931
95. Ikeda S, Toganoh M, Easwaramoorthi S, Lim JM, Kim D, Furuta H (2010) J Org Chem 75:8637–8649
96. Fujino K, Hirata Y, Kawabe Y, Morimoto T, Srinivasan A, Toganoh M, Miseki Y, Kudo A, Furuta H (2011) Angew Chem Int Ed 50:6855–6859
97. Wei PC, Zhang K, Li X, Meng DY, Ågren H, Ou ZP, Ng S, Furuta H, Xie YS (2014) Angew Chem Int Ed 53:14069–14073
98. Lindsey JS, Mass O, Chen C-Y (2011) New J Chem 35:511–516
99. Yang EY, Kirmaier C, Krayer M, Taniguchi M, Kim H-J, Diers JR, Bocian DF, Lindsey JS, Holten D (2011) J Phys Chem B 115:10801–10816
100. Chen C-Y, Sun EJ, Fan DZ, Taniguchi M, McDowell BE, Yang EK, Diers JR, Bocian DF, Holten D, Lindsey JS (2012) Inorg Chem 51:9443–9464
101. Vairaprakash P, Yang E, Sahin T, Taniguchi M, Krayer M, Diers JR, Wang A, Niedzwiedzki DM, Kirmaier C, Lindsey JS, Bocian DF, Holten D (2015) J Phys Chem B 119:4382–4395
102. Muthiah C, Kee HL, Diers JR, Fan DZ, Ptaszek M, Bocian DF, Holten D, Lindsey JS (2008) Photochem Photobiol 84:786–801
103. Kee HL, Nothdurft R, Muthiah C, Diers JR, Fan DZ, Ptaszek M, Bocian DF, Lindsey JS, Culver JP, Holten D (2008) Photochem Photobiol 84:1061–1072
104. Crossley MJ, Burn PL (1991) J Chem Soc Chem Commun 1569–1571
105. Tsuda A, Osuka A (2001) Science 293:79–82
106. Bonifazi D, Scholl M, Song FY, Echegoyen L, Accorsi G, Armaroli N, Diederich F (2003) Angew Chem Int Ed 42:4966–4970
107. Cho HS, Jeong DH, Cho S, Kim D, Matsuzaki Y, Tanaka K, Tsuda A, Osuka A (2002) J Am Chem Soc 124:14642–14654
108. Frampton MJ, Accorsi G, Armaroli N, Rogers JE, Fleitz PA, McEwan KJ, Anderson HL (2007) Org Biomol Chem 5:1056–1061
109. Pawlicki M, Morisue M, Davis NKS, McLean DG, Haley JE, Beuerman E, Drobizhev M, Rebane A, Thompson AL, Pascu SI, Accorsi G, Armaroli N, Anderson HL (2012) Chem Sci 3:1541–1547
110. Diev VV, Schlenker CW, Hanson K, Zhong QW, Zimmerman JD, Forrest SR, Thompson ME (2012) J Org Chem 77:143–159
111. Jiao CJ, Huang K-W, Guan Z, Xu Q-H, Wu J (2010) Org Lett 12:4046–4049
112. Sessler JL, Johnson MR (1987) Angew Chem Int Ed Engl 26:678–680
113. Iehl J, Vartanian M, Holler M, Nierengarten J-F, Delavaux-Nicot B, Strub J-M, Van Dorsselaer A, Wu YL, Mohanraj J, Yoosaf K, Armaroli N (2011) J Mater Chem 21:1562–1573
114. Armaroli N, Accorsi G, Song FY, Palkar A, Echegoyen L, Bonifazi D, Diederich F (2005) ChemPhysChem 6:732–743
115. Duncan TV, Susumu K, Sinks LE, Therien MJ (2006) J Am Chem Soc 128:9000–9001
116. Chang M-H, Hoffmann M, Anderson HL, Herz LM (2008) J Am Chem Soc 130:10171–10178
117. Hoffmann M, Kärnbratt J, Chang M-H, Herz LM, Albinsson B, Anderson HL (2008) Angew Chem Int Ed 47:4993–4996
118. Sprafke JK, Kondratuk DV, Wykes M, Thompson AL, Hoffmann M, Drevinskas R, Chen W-H, Yong CK, Karnbratt J, Bullock JE, Malfois M, Wasielewski MR, Albinsson B, Herz LM, Zigmantas D, Beljonne D, Anderson HL (2011) J Am Chem Soc 133:17262–17273
119. Rousseaux SAL, Gong JQ, Haver R, Odell B, Claridge TDW, Herz LM, Anderson HL (2015) J Am Chem Soc 137:12713–12718
120. Parkinson P, Knappke CEI, Kamonsutthipaijit N, Sirithip K, Matichak JD, Anderson HL, Herz LM (2014) J Am Chem Soc 136:8217–8220
121. Isago H (2015) Optical spectra of phthalocyanines and related compounds. A guide for beginners. Springer, Tokyo
122. Ragoussi M-E, Ince M, Torres T (2013) Eur J Org Chem 2013:6475–6489
123. Singh S, Aggarwal A, Bhupathiraju NVSDK, Arianna G, Tiwari K, Drain CM (2015) Chem Rev 115:10261–10306
124. Rio Y, Rodriguez-Morgade MS, Torres T (2008) Org Biomol Chem 6:1877–1894
125. Kobayashi N, Ogata H, Nonaka N, Luk'yanets EA (2003) Chem Eur J 9:5123–5134
126. Łapok Ł, Obłoza M, Gorski A, Knyukshto V, Raichyonok T, Waluk J, Nowakowska M (2016) ChemPhysChem 17:1123–1135

127. Soldatova AV, Kim J, Rizzoli C, Kenney ME, Rodgers MAJ, Rosa A, Ricciardi G (2011) Inorg Chem 50:1135–1149
128. Kim J, Soldatova AV, Rodgers MAJ, Kenney ME (2013) Polyhedron 57:64–69
129. Borisov SM, Zenkl G, Klimant I (2010) ACS Appl Mater Interfaces 2:366–374
130. Ho C-L, Li H, Wong W-Y (2014) J Organomet Chem 751:261–285
131. Zhang KY, Liu SJ, Zhao Q, Li FY, Huang W (2015) In: Lo KK-W (ed) Luminescent and photoactive transition metal complexes as biomolecular probes and cellular reagents, structure and bonding, vol 165, pp 131–180
132. Kumar A, Sun SS, Lees AJ (2010) In: Lees AJ (ed) Photophysics of organometallics, topics in organometallic chemistry, vol 29, pp 1–35
133. Kirgan RA, Sullivan BP, Rillema DP (2007) In: Balzani V, Campagna S (eds) Photochemistry and photophysics of coordination compounds II, topics in current chemistry, vol 281, pp 45–100
134. Worl LA, Duesing R, Chen PY, Dellaciana L, Meyer TJ (1991) J Chem Soc Dalton Trans 849–858
135. Tapolsky G, Duesing R, Meyer TJ (1990) Inorg Chem 29:2285–2297
136. Caspar JV, Sullivan BP, Meyer TJ (1984) Inorg Chem 23:2104–2109
137. Yam VW-W, Lau VC-Y, Cheung K-K (1995) Organometallics 14:2749–2753
138. Villegas JM, Stoyanov SR, Huang W, Rillema DP (2005) Dalton Trans 1042–1051
139. Villegas JM, Stoyanov SR, Huang W, Rillema DP (2005) Inorg Chem 44:2297–2309
140. Yu T, Tsang DP-K, Au VK-M, Lam WH, Chan M-Y, Yam VW-W (2013) Chem Eur J 19:13418–13427
141. Balzani V, Juris A, Venturi M, Campagna S, Serroni S (1996) Chem Rev 96:759–833
142. Campagna S, Puntoriero F, Nastasi F, Bergamini G, Balzani V (2007) In: Balzani V, Campagna S (eds) Photochemistry and photophysics of coordination compounds I, topics in current chemistry, vol 280, pp 117–214
143. Chi Y, Chou P-T (2007) Chem Soc Rev 36:1421–1431
144. Kumaresan D, Shankar K, Vaidya S, Schmehl RH (2007) In: Balzani V, Campagna S (eds) Photochemistry and photophysics of coordination compounds II, topics in current chemistry, vol 281, pp 101–142
145. Sauvage J-P, Collin J-P, Chambron J-C, Guillerez S, Coudret C, Balzani V, Barigelletti F, De Cola L, Flamigni L (1994) Chem Rev 94:993–1019
146. Carlson B, Phelan GD, Kaminsky W, Dalton L, Jiang XZ, Liu S, Jen AK-Y (2002) J Am Chem Soc 124:14162–14172
147. Caspar JV, Meyer TJ (1983) J Phys Chem 87:952–957
148. Bergman SD, Gut D, Kol M, Sabatini C, Barbieri A, Barigelletti F (2005) Inorg Chem 44:7943–7950
149. Bergman SD, Goldberg I, Barbieri A, Kol M (2005) Inorg Chem 44:2513–2523
150. Bergman SD, Goldberg I, Barbieri A, Barigelletti F, Kol M (2004) Inorg Chem 43:2355–2367
151. Lee T-C, Hung J-Y, Chi Y, Cheng Y-M, Lee G-H, Chou P-T, Chen C-C, Chang C-H, Wu C-C (2009) Adv Funct Mater 19:2639–2647
152. Kalyanasundaram K (1992) Photochemistry of polypyridine and porphyrin complexes. Academic Press, London
153. Matar F, Ghaddar TH, Walley K, DosSantos T, Durrant JR, O'Regan B (2008) J Mater Chem 18:4246–4253
154. Damas A, Gullo MP, Rager MN, Jutand A, Barbieri A, Amouri H (2013) Chem Commun 49:3796–3798
155. Tung Y-L, Lee S-W, Chi Y, Chen L-S, Shu C-F, Wu F-I, Carty AJ, Chou P-T, Peng S-M, Lee G-H (2005) Adv Mater 17:1059–1064
156. Abrahamsson M, Jäger M, Kumar RJ, Österman T, Persson P, Becker H-C, Johansson O, Hammarström L (2008) J Am Chem Soc 130:15533–15542
157. Abrahamsson M, Jäger M, Österman T, Eriksson L, Persson P, Becker H-C, Johansson O, Hammarström L (2006) J Am Chem Soc 128:12616–12617
158. Montalti M, Credi A, Prodi L, Gandolfi MT (2006) Handbook of photochemistry, 3rd edn. CRC Press, FL, pp 617–633
159. Flamigni L, Barbieri A, Sabatini C, Ventura B, Barigelletti F (2007) Photochemistry and photophysics of coordination compounds II, topics in current chemistry, vol 281, pp 143–203
160. Djurovich PI, Thompson ME (2007) In: Yersin H (ed) Highly efficient OLEDs with phosphorescent materials, Wiley, Weinheim, pp 131–161

161. Tsuboyama A, Okada S, Ueno K (2007) In: Yersin H (ed) Highly efficient OLEDs with phosphorescent materials, Wiley, Weinheim, pp 163–183
162. Chen H-Y, Yang C-H, Chi Y, Cheng Y-M, Yeh Y-S, Chou P-T, Hsieh H-Y, Liu C-S, Peng S-M, Lee G-H (2006) Can J Chem 84:309–318
163. Polson M, Ravaglia M, Fracasso S, Garavelli M, Scandola F (2005) Inorg Chem 44:1282–1289
164. Williams JAG (2007) In: Balzani V, Campagna S (eds) Photochemistry and photophysics of coordination compounds II, topics in current chemistry, vol 281, pp 205–268
165. Adams CJ, Fey N, Harrison ZA, Sazanovich IV, Towrie M, Weinstein JA (2008) Inorg Chem 47:8242–8257
166. Paw W, Cummings SD, Mansour MA, Connick WB, Geiger DK, Eisenberg R (1998) Coord Chem Rev 171:125–150
167. Cummings SD, Eisenberg R (1996) J Am Chem Soc 118:1949–1960
168. Kozhevnikov DN, Kozhevnikov VN, Shafikov MZ, Prokhorov AM, Bruce DW, Williams JAG (2011) Inorg Chem 50:3804–3815
169. Yam VW-W, Chan KH-Y, Wong KM-C, Zhu N (2005) Chem Eur J 11:4535–4543
170. Michalec JF, Bejune SA, McMillin DR (2000) Inorg Chem 39:2708–2709
171. Baik C, Han W-S, Kang Y, Kang SO, Ko J (2006) J Organomet Chem 691:5900–5910
172. Chan C-W, Lai T-F, Che C-M, Peng S-M (1993) J Am Chem Soc 115:11245–11253
173. Cocchi M, Virgili D, Fattori V, Williams JAG, Kalinowski J (2007) Appl Phys Lett 90:023506
174. Rossi E, Murphy L, Brothwood PL, Colombo A, Dragonetti C, Roberto D, Ugo R, Cocchi M, Williams JAG (2011) J Mater Chem 21:15501–15510
175. Yam VW-W, Cheng EC-C (2007) In: Balzani V, Campagna S (eds) Photochemistry and photophysics of coordination compounds II, topics in current chemistry, vol 281, pp 269–309
176. To W-P, Tong GS-M, Lu W, Ma CS, Liu J, Chow AL-F, Che C-M (2012) Angew Chem Int Ed 51:2654–2657
177. Sculfort S, Braunstein P (2011) Chem Soc Rev 40:2741–2760
178. Armaroli N, Accorsi G, Cardinali F, Listorti A (2007) In: Balzani V, Campagna S (eds) Photochemistry and photophysics of coordination compounds I, topics in current chemistry, vol 280, pp 69–115
179. Armaroli N (2001) Chem Soc Rev 30:113–124
180. Shan X-c, Jiang F-l, Yuan D-q, Zhang H-b, Wu M-y, Chen L, Wei J, Zhang S-q, Pan J, Hong M-c (2013) Chem Sci 4:1484–1489
181. Tsuge K, Chishina Y, Hashiguchi H, Sasaki Y, Kato M, Ishizaka S, Kitamura N (2016) Coord Chem Rev 306:636–651
182. Ford PC, Cariati E, Bourassa J (1999) Chem Rev 99:3625–3647
183. Kyle KR, Ryu CK, Di Benedetto JA, Ford PC (1991) J Am Chem Soc 113:2954–2965